Low-temperature terahertz spectroscopy of $LaFeO_3$, $PrFeO_3$, $ErFeO_3$, and $LuFeO_3$: Quasimagnon resonances and ground-state multiplet transitions

Néstor E. Massa,[1,*] Leire del Campo,[2] Vinh Ta Phuoc,[3] Paula Kayser,[4,†] and José Antonio Alonso[5]

[1]*Centro CEQUINOR, Consejo Nacional de Investigaciones Científicas y Técnicas, Universidad Nacional de La Plata, Bv. 120 1465, B1904 La Plata, Argentina*

[2]*Centre National de la Recherche Scientifique, CEMHTI UPR3079, Université Orléans, F-45071 Orléans, France*

[3]*Groupement de Recherche Matériaux Microélectronique Acoustique Nanotechnologies-UMR 7347 CNRS, Université de Tours, INSA CVL, Parc Grandmont F-37200, TOURS, France*

[4]*Centre for Science at Extreme Conditions and School of Chemistry, University of Edinburgh, Kings Buildings, Mayfield Road, EH9 3FD Edinburgh, United Kingdom*

[5]*Instituto de Ciencia de Materiales de Madrid, Consejo Superior de Investigaciones Científicas (CSIC), Cantoblanco, E-28049 Madrid, Spain*

(Received 24 August 2022; revised 3 May 2023; accepted 4 August 2023; published 8 September 2023)

We report on zone center terahertz excitations of non-Jahn Teller $LaFeO_3$, $PrFeO_3$, $ErFeO_3$, and $LuFeO_3$ distorted perovskites under external magnetic fields up 7 T. Our measurements on low-temperature/low-energy absorptions of $LaFeO_3$ show quasiantiferromagnetic (q-AFM) and quasiferromagnetic (q-FM) magnons at $\omega_{q\mathrm{AFM}} \sim 31.4\ \mathrm{cm}^{-1}$ and $\omega_{q\mathrm{FM}} \sim 26.7\ \mathrm{cm}^{-1}$ in the Γ_4 (G_x, A_y, F_z) representation with near degeneracy linearly lifted by the field. $LuFeO_3$ is characterized by zero-field magnetic resonances at $\omega_{q\mathrm{AFM}} \sim 26.3\ \mathrm{cm}^{-1}$ and $\omega_{q\mathrm{FM}} \sim 22.4\ \mathrm{cm}^{-1}$ in addition to Fe^{3+} Zeeman-split crystal field (CF) $6A_1$ ground transitions at $\sim 10.4\ \mathrm{cm}^{-1}$ triggered by subtle structural deviations induced by the Lu $4f^14$ smaller ionic radius at the A site. This local quasinoncentrosymmetric departure is also found in $ErFeO_3$ (Kramers $4f^{11}$ Er^{3+} ($^4I_{15/2}$); $\Gamma_2(F_x, C_y, G_z) < T_{\mathrm{SR}} \sim 93$ K) but with the $\sim 4\ \mathrm{cm}^{-1}$ Fe^{3+} Zeeman branching strongly biased toward higher energies due to $3d$-$4f$ exchange. Magnons at $\omega_{q\mathrm{AFM}} \sim 31.5\ \mathrm{cm}^{-1}$ and $\omega_{q\mathrm{FM}} \sim 21.5\ \mathrm{cm}^{-1}$ in $ErFeO_3$ do not undergo field-induced band splits but a 13-fold increase in the q-AFM ($\omega_{q\mathrm{AMF}}$)/q-FM ($\omega_{q\mathrm{AFM}}$) intensity ratio. There is a remarkable field-dependent CF matching population balance between Fe^{3+} higher and Er^{3+} lower Zeeman branches. The Er^{3+} ($^4I_{15/2}$) multiplet, at the 49.5, 110.5, and 167.3 cm^{-1}, coincides with external lattice mode frequencies, suggesting strong lattice-driven spin-phonon interactions. Far-infrared absorption ratios under mild external fields reveal magnetic dependence only for those zone-center phonons involving moving magnetic ions. Overall, our results support the viability of magnetic state manipulation by phonons. Quasiantiferroresonances and quasiferroresonances in $PrFeO_3$ turn much broader as non-Kramers Pr^3 introduces ligand changes at the A site, leading into near degeneracy the q-AFM mode and the lowest Pr^{3+} CF transition. They merge into a single broad mostly unresolved feature at 7 T. We conclude that low-energy excitations in $RFeO_3$ (R = rare earth) strongly depend on the lanthanide ionic size, thus indivisibly tied to the mechanism associated with the origin of canted FM. In addition, minute lattice displacements also underlie considering noncentrosymmetric the most distorted $RFeO_3$ (R = rare earth). In these perovskites, the changes triggered in the lattice by the smaller rare earth and the nonlinear intrinsic oxygen ion polarizability, known to drive lattice instabilities, provide grounds for interplay of ionic and electronic interactions yielding ferroelectric spontaneous polarization.

DOI: 10.1103/PhysRevB.108.115116

I. INTRODUCTION

The search for multifunctional materials with magnetic and electronic polarizations as in ferromagnetic (FM) ferroelectric multiferroics [1] has contributed in the last decades to advances in material development aiming at devices that would potentially perform more than one task [2]. Here, $RFeO_3$ (R = rare earth) is one family of these compounds sustaining a distorted cubic perovskite lattice. Increasing the degree of octahedral tilting across the series was recognized early to accommodate structural distortions and interplays in a unique magnetic and electronic environment created by the Fe^{3+} and R^{3+} ions [3–6]. These cooperative exchanges may then be incorporated into developments that would change our way of life as in the proposed magnetizable concrete for road electrification aimed at vehicle on-the-road charging [7].

The rich magnetic phase diagram of $RFeO_3$ originates in the Fe^{3+} and R^{3+} independent magnetic sublattices containing Fe^{3+} canted spins tangled in the magnetic order of iron and $4f$ lanthanide exchanges promoting magnetoelectric

*neemmassa@gmail.com

†Present address: Departamento de Química Inorgánica, Facultad de Ciencias Químicas, Universidad Complutense de Madrid, 28040 Madrid, Spain.

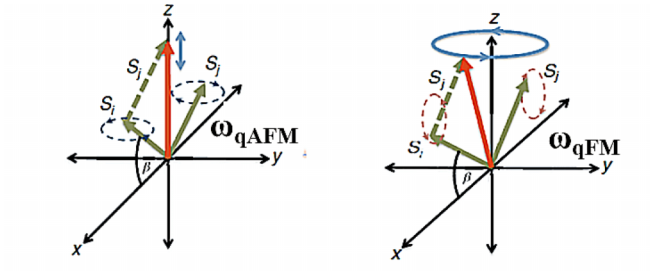

(a) Quasiantiferromagnetic spin mode (b) Quasiferromagnetic spin mode

FIG. 1. Low-energy resonant modes for antiferromagnets: (a) higher-energy quasiantiferromagnetic ($\omega_{q\mathrm{AFM}}$) resonance built on x, y out-of-phase oscillations and in-phase oscillations along the z axis; (b) quasiferromagnetic ($\omega_{q\mathrm{FM}}$) resonance named after the distorted low-frequency cone defined by the ferromagnetic moment precessing the z axis. After Herrmann [24] and Constable *et al.* [35].

couplings. The consequences of this appear as changes in phonon transverse optical–longitudinal optical (TO-LO) macroscopic field magnetic and electric dependences [8,9], Heisenberg magnons [10], crystal field (CF) levels, and in Fe^{3+} canted magnons within the spectral region from far-infrared to the terahertz.

Here, $R\mathrm{FeO_3}$ ferrites, with four molecules per unit cell ($Z = 4$), belong to the room-temperature crystalline space group $Pbmn$ (D_{2h}^{16}) [11] with Fe^{3+} $3d^5$ in a $S = \frac{5}{2}$ spin-moment high-state configuration. Below their Néel temperatures T_N [12], Fe^{3+} is centrally located in a cage made of six antiparallel nearest neighbors facing each other in an isotropic antiferromagnetic (AFM) coupling. This represents the strongest magnetic interaction in the type-G plane arrangement of the Γ_4 (G_x, A_y, F_z) representation, meaning a G_x AFM ground state along the a axis, an A_y weak AFM along the b axis, and a F_z weak canted FM along the c axis [13,14]. Next in strength is the Fe^{3+}-R^{3+} exchange followed by the weaker AFM R^{3+}-R^{3+} interaction found at low temperatures when paramagnetic rare-earth moments turn ordered in an environment of complex exchanges that may include exchange-mediated out-of-ac-plane magnetic components as in the Γ_1 (A_x, G_y, C_z) representation (Fig. S1 in the Supplemental Material [15]).

The distinctive F_z FM component in Γ_4 (G_x, A_y, F_z) along the c axis originates in noncollinear spin canting with out-of-plane deviations of the order of $< 1^\circ$. Regardless of the prevalent mechanism for the origin of canted FM, either from Dzyalonshinkii-Moriya antisymmetric spin exchanges [16,17] or rare-earth-induced lattice anisotropies [18], existing R^{3+} moments always have a finite exchange within Fe^{3+} CF in the octahedral sublattice [19]. This triggers spontaneous reorientation (SR) of the iron moments when the field is just large enough to pull the net moment parallel to the c axis [20], and as consequence, a nonzero f-R^{3+}–rare-earth magnetic moment and d-M^{3+} transition metal exchange reorients, on, G antiferromagnetism and canted ferromagnetism from room-temperature Γ_4 (G_x, A_y, F_z) to the lower-temperature representation Γ_2 (F_x, C_y, G_z) [21,22].

Low-energy spin-wave Fe^{3+} magnetic excitations (Fig. 1) are zone-center precession modes associated with canting that appear in the terahertz as weak absorptions when stimulated by the infrared light ac magnetic field. They are named in orthorhombic distorted perovskites quasiantiferromagnetic (q-AFM; $\omega_{q\mathrm{AMF}}$) and quasiferromagnetic (q-FM; $\omega_{q\mathrm{FM}}$) modes detectable when the oscillating frequency of the light matches the zone-center frequency of spin-wave cooperative motions [23]. Each resonance is coupled to an exchange mode so that their optical activity is not confined to a specified crystallographic direction, and thus, they should not be viewed as normal modes [24]. One mode ($\omega_{q\mathrm{AFM}}$) depends on anisotropies in the ac plane along the AFM axis, with the spin net sum in this plane, while the other ($\omega_{q\mathrm{FM}}$) aligns along the FM c axis, performing the net spin rocking motion following the motion of the sublattice spins [25,26].

Kittel [27], Nagamiya [28], and Keffer and Kittel [29] addressed these $k \approx 0$ magnon resonances with a simplifying approach in which room-temperature Γ_4 (A_y) and low-temperature Γ_2 (C_y) spin deviations were neglected. This results in a *de facto* reduction of the inequivalent number of molecules per unit cell in the magnetic structure from four magnetic sublattices of the d subsystem $M_i (i = 1, \ldots, 4)$ and four rare-earth sublattices m_j ($j = 1, \ldots, 4$) to two with individual Fe^{3+} magnetic moments M_j ($j = 1$–4) bound by the equivalencies $M_1 = M_3$ and $M_2 = M_4$ in the so-called two-sublattice approximation. Accordingly, each magnetization from the two magnetic sublattices along narrow optical orbitals is named M_1 and M_2 and has its equation of motion linked by an exchange interaction that describes unequal precessions triggering the two resonant energy modes function of exchange and anisotropy fields in the orthorhombic lattice [29].

These collective spin excitations have been widely studied by many material research groups working with noncollinear AFMs [24,25]. Among them, White *et al.* [26] and Koshizuka *et al.* [30,31] reported temperature-dependent Raman scattering of $YFeO_3$, $SmFeO_3$, $DyFeO_3$, $HoFeO_3$, and $ErFeO_3$, and Koslov *et al.* [32] pioneered terahertz techniques measuring $R\mathrm{FeO_3}$ (R = Y, Tm, Dy, Gd, Ho, Er, Tb). Resonant optical pumping of f-f electronic transitions of Dy^{3+} in AFM $DyFeO_3$ was reported to strongly affect the induced magnetization dynamics that is intrinsically competing with the Fe^{3+} off-resonant excitation of the subsystem spin waves [33].

Constable *et al.* [34] and Jiang *et al.* [35] studied the temperature-dependent spin waves and neutron scattering and spin reorientation in $NdFeO_3$, respectively; Fu *et al.* [36] measured spin resonances in $SmFeO_3$, and Zhang *et al.* [37] did it in $TmFeO_3$ using terahertz time-domain spectroscopy. Also, $YFeO_3$ zone-center two-spin wave modes have been studied up to17 T by Amelin *et al.* [38], and Li *et al.* [39] proposed a study on cooperative exchange coupling of a spin ensemble in Y-doped $ErFeO_3$. More recently, the spin dynamics of $TmFeO_3$ [40] and $TbFeO_3$ [41] have been addressed by neutron spectroscopies.

Changing the magnetic anisotropy for Fe^{3+} spins by resonant terahertz pumping of electronic orbital transitions in$TmFeO_3$ was found to trigger large-amplitude coherent oscillations [42]. It has been further demonstrated that, in $TmFeO_3$, coherent pulse steering of spins may be achieved by antenna terahertz picosecond electric fields coupling spin-switching selected states by external magnetic fields [43].

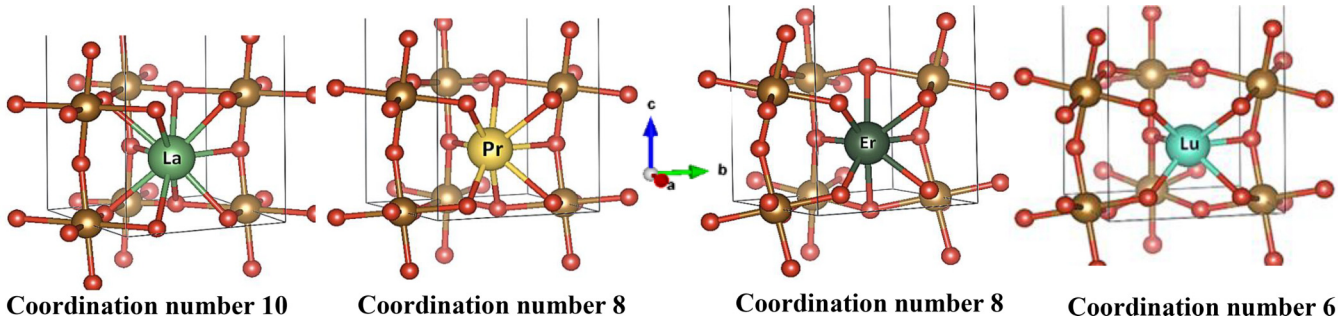

FIG. 2. Change of rare-earth coordination number in the orthorhombic perovskite polyhedral A site as the lanthanide ionic radius decreases from La^{3+} to Lu^{3+} distorting the higher-temperature cubic phase AO_{12} cage [11,44,45,47,48].

The low-energy spin-precession modes share the terahertz spectral region with transition metal CF ground transitions linked to local distortions and sublattice tilted angles that in turn also depend on less-prone-to-modify chemical bond rare earths.

Early diffraction measurements on $R\mathrm{FeO_3}$ (R = rare earth) ferrites [11,44,45] showed that the A polyhedral sites have an anomalous decrease in the number of rare-earth–oxygen nearest neighbors that, deviating from the higher-temperature cubic phase AO_{12} cage, changes from 10 in $LaFeO_3$ to 6 in $LuFeO_3$ (Fig. 2). The reduction of the Fe-O-Fe θ bond angle from 157 ° in $LaFeO_3$ to 142 ° in $LuFeO_3$ implies subtle changes in orbital and spin ordering [46–50] that is mirrored in the Néel temperature depending linearly on the Fe-O-Fe superexchange angle and thus on the rare-earth cation size [51].

The proven lattice ductility of distorted perovskites has profound implications for enabling B-site CF symmetry-forbidden Fe^{3+} transitions of the $^6A_1$ multiplet. As we detail in the following sections, Fe^{3+} ground-state Zeeman split transitions are a distinctive feature of the $LuFeO_3$ terahertz spectra that weigh additionally to the sole spin-mode picture found in $LaFeO_3$ that, having a lattice closer to cubic, prevents Fe^{3+} CF transitions becoming optically active. Although both compounds nominally share the *Pbnm* (D_{2h}^{16}) space group, the Fe^{3+} site point group in $LuFeO_3$ is altered by the ligand distortions due to Lu^{3+} smaller ionic radius in a cage with only net six Lu-O nearest neighbors creating noncentrosymmetric subtle deformations in Fe^{3+}-O ligands.

This Fe^{3+} CF Zeeman branching in $LuFeO_3$ has as a counterpart in the $ErFeO_3$ Er^{3+} ($^4I_{15/2}$) multiplet split which is strongly biased due to iron–rare-earth exchanges. The Er^{3+} ($^4I_{15/2}$) CF also overlaps with specific lattice phonons, suggesting conspicuous spin-phonon interactions appearing as an induced local continuum through the Er-O lattice vibrational range in the 1 T/0 T far-infrared ratios. Weak applied fields are also enough to hint at variants in partially magnetic-driven reststrahlen associated with torsional LO-mode macroscopic fields involving moving Fe^{3+} ions.

While spin resonances under applied magnetic fields vary from characteristic enhancements to near CF degeneracies, we conclude that the overall complex setting, also undergoing some degree of lattice electric and magnetic coupling in a scenario prone to localized polaron formation, is a likely common to all ferrite oxides.

II. SAMPLE PREPARATION AND STRUCTURAL CHARACTERIZATION

$R\mathrm{FeO_3}$ (R = La, Pr, Er, Lu) polycrystalline samples were prepared by standard ceramic synthesis procedures. Stoichiometric amounts of analytical grade Fe_2O_3 and R_2O_3 powder oxides were thoroughly ground and heated in air at 1000 °C for 12 h and 1300 °C for 12 h in alumina crucibles. Then pellets of ∼1 cm diameter, < 2 mm thick, were prepared by uniaxial pressing the raw powders and sintering the disks at 1300 °C for 2 h. The purity of the samples for all four $R\mathrm{FeO_3}$ (R = La, Pr, Er, Lu) samples was checked by x-ray powder diffraction (XRD) collected at room temperature with Cu-$K\alpha$ radiation. Shown in Fig. S2 in the Supplemental Material [15], all data were analyzed using the Rietveld method with refinements carried out with FULLPROF.

III. EXPERIMENTAL DETAILS

Low-temperature–low-frequency absorption measurements in the spectral range from 3 to 50 cm^{-1} with 0.5 cm^{-1} resolution have been performed in the terahertz beamline of the BESSY II storage ring at the Helmholtz-Zentrum Berlin (HZB) in the low-α multibunch hybrid mode [56].

In the synchrotron low-α mode, electrons are compressed within shorter bunches of only ∼2 ps duration, allowing far-infrared wave trains up to milliwatt average power to overlap coherently in the terahertz range < 50 cm^{-1} [57,58].

For measurements under magnetic fields, we used a superconducting magnet (Oxford Spectromag 4000, here up 7.5 T) interfaced with a Bruker IFS125 HR interferometer (Fig. S3 in the Supplemental Material [15]). Temperatures were measured with a calibrated Cernox Sensor from LakeShore Cryotronics mounted to the copper block that holds the sample in the magnet variable temperature insert. Liquid-helium-cooled Si bolometers (4.2 and 1.6 K from Infrared Labs) were used as detectors [15]. All measurements have been done in the Voigt configuration. We have also used $ErFeO_3$ powder-embedded polyethylene pellets in the beamline facilities to identify Er^{3+} multiplet and phonon field dependences in the far-infrared by calculating the ratio of $ErFeO_3$ spectra under 1 Tesla against that zero-field cooled (ZFC) at 5 K.

Far-infrared near-normal reflectivity spectra were taken on heating from 4 to 300 K at 1 cm^{-1} resolution with Bruker 113V and Bruker 66 interferometers with conventional near-

normal incidence geometry. Samples were mounted on the cold finger of a He-closed-cycle refrigerator and a homemade He cryostat adapted to the near-normal reflectivity attachment vacuum chamber of the interferometer. A He-cooled bolometer and a deuterated triglycine sulfate pyroelectric bolometer were employed to completely cover the spectral range of interest. A plain gold mirror and *in situ* evaporated gold film were used for 100% reference reflectivity between 4 and 300 K. We analyzed the reflectivity spectra using the standard procedures for multioscillator dielectric simulation [59–61].

IV. RESULTS AND DISCUSSION

A. $LaFeO_3$

Sharing the space group with the rest of the $RFeO_3$ (R = lanthanide and Y) ferrites, 4-molecules-per-unit-cell $LaFeO_3$ is the simplest compound that, while closest to the cubic structure [50], still adopts the $Pbnm$-D_{2h}^{16} orthorhombic space group [62–65].

Here, G-type $LaFeO_3$ has spins coupled strongly AFM below $T_N \sim 740$ K [66] in high-spin-configuration Fe^{3+} (half-filled $3D^5$) $S = \frac{5}{2}$. Inelastic neutron scattering spin-wave intensities were found well represented by the Heisenberg exchange interaction between nearest-neighbor AFM planes prompting a van Hove singularity at $\sim$564 cm^{-1} in the density of states spawning from 323 to 630 cm^{-1} [66].

At lower frequencies, as pointed at in the Introduction, work on long-wavelength spin waves has mostly been done under the umbrella of the so-called two-sublattice approximation [30] that considers spins 1–3 and 2–4 equivalent with each sublattice magnetization M_1 and M_2, having its own equation of motion linked to the exchange interaction describing unequal precessions. The resonant energies then are given as

$$\hbar|\omega_k^{\pm}| = g\mu_B[H_A(2H_E + H_A)^2]^{1/2} + g\mu_B H_0, \qquad (1)$$

where H_A is an effective anisotropy field, $H_E = 2|J|zS/g\mu_B(H_{Ei} = \lambda M_i,\ i = 1,\ 2)$ with the exchange interaction J only for nearest-neighbor spins, S is the spin moment of the ith and jth nearest-neighbor metal transition ions, and g is the gyromagnetic ratio as the spectroscopic splitting factor [67]. A more quantitative treatment describing the terahertz active q-FM and q-AFM zone-center spin-wave resonances needs a full Hamiltonian incorporating anisotropies. The conventional spin Hamiltonian for orthorhombic ferrites [24,25,27,35] is then written considering a single isotropic exchange constant coupling nearest-neighbor transition metal spins, a single antisymmetric (canting) exchange constant, and two anisotropy constants as in

$$H_{spin} = 2J\sum_{i,j} S_i S_j + \sum_{i,j} D\,(S_i S_j) + \sum_{i,j} (K_{eff} S_i)^2. \qquad (2)$$

We thus expect a relatively weak resonant long-wavelength pair with near-equal intensity and comparable temperature and magnetic field dependences near the Brillouin zone center. These, Fig. 1, are given by

$$\omega_{qFM} = \{24JS[2(K_a - K_c)S]\}^{1/2}, \qquad (3)$$

$$\omega_{qAFM} = [24JS(6DS\tan\beta + 2K_a S)]^{1/2}, \qquad (4)$$

with the q-AFM (ω_{qAFM}) resonance at higher energies than the corresponding q-FM (ω_{qFM}), J being the exchange integral (J is positive for FMs and negative for AFMs), the isotropic Heisenberg constant, and D the antisymmetric (DM) constant, S is the spin moment of the ith and jth nearest-neighbor metal transition ions, and K_a and K_c are anisotropies along the a and c axes. Here, β is the momentum canting angle off the ab plane [68].

Figure 3(a) shows the $LaFeO_3$ q-FM (ω_{qFM}) and q-AFM (ω_{qAFM}) zone-center active resonances that, normalized by the absorption spectrum at 110 K, undergo a monotonous cooling down to 2.4 K. The lower- and upper-energy modes have frequencies peaking at $\omega_{qFM} = 14.7$ cm^{-1} and $\omega_{qAFM} = 20.1$ cm^{-1}, respectively. They are near temperature independent, corroborating that, by having a La ($4f^0$) closed shell, avoiding extra potentially disturbing rare-earth exchange, $LaFeO_3$ holds below-T_N G-type magnetism in the Γ_4 (G_x, A_y, F_z) [67,69–71] representation with canting angle α (deg.) ~ 0.52 [72]. These resonances are found even in the absence of an external field B_0, with energy dependences fixed by exchange and anisotropy fields. We found that our peak positions are also in agreement with lower-resolution inelastic neutron scattering measurements reporting broad features at those frequencies [73].

Applying an external field B_0 means that both modes will no longer remain degenerate since, if one resonant mode is close to parallel to the applied effective field, the second has the opposite sign so that the resulting picture is a diverging split [30]. We find this behavior fully reproduced in our measurements of $LaFeO_3$ q-FM- and q-AFM-like modes, as increasing applied field breaks their zone-center degeneracy. This also reassures that our ZFC excitations have magnetic origin (Fig. S4 in the Supplemental Material [15]).

We compute the induced modifications in zone-center absorptions by the applied field B_0 by normalizing the measured spectra using the ZFC run (Fig. 4). These ratios ($B_{0J}/0.0T$) yield an absolute account of the bulk field-dependent spectral changes. The ω_{qAFM} magnon initially peaks in intensity and remains unresolved up to $\sim$3 T, meaning that this narrower band is the result of two superposing excitations that remain unresolved at our working 0.5 cm^{-1} resolution. At higher fields, it divides into two components. On the other hand, the q-FM-like mode ω_{qFM} shows only a gentle gradual splitting and broadening $>$ 3 T. At 1 T, Fig. S5 in the Supplemental Material [15], it may be further deconvoluted into two bands, a Gaussian now centered at $\sim$11.6 cm^{-1} and another much broader asymmetric at $\sim$16.9 cm^{-1} with a truncated peak profile in the 1–3 T range, under a Gaussian multiconstituent envelope, that may be understood as due to the disruption of individual magnetic sites by the external field perhaps heightened due to the polycrystalline character of our samples. This resonance becomes narrower and comparable with the other magnetic bands increasing fields, all conforming under 7 T a close frequency quartet at 22.8, 21.3, 17.15 and 11.1 cm^{-1} [Fig. 4 (inset)], suggesting that the low-field broadening is

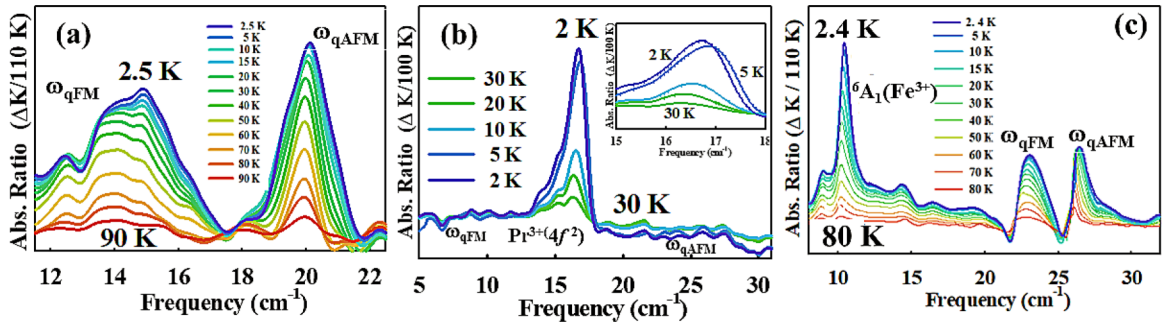

FIG. 3. (a) Zone-center temperature quasiantiferromagnetic (q-AFM; $\omega_{q\mathrm{AFM}}$) and quasiferromagnetic (q-FM; $\omega_{q\mathrm{FM}}$) magnon modes of $LaFeO_3$ using the 110 K spectrum as normalizing reference. (b) Zone-center temperature-dependent first excited state of the $Pr^{3+}(4f^2)$ $^3H_4$ manifold and weaker side bands assigned to the $\omega_{q\mathrm{AFM}}$ and $\omega_{q\mathrm{FM}}$ resonances in $PrFeO_3$ using the 110 K spectrum as normalizing reference. Inset: Details showing the undergoing peak softening in the 5 to ∼2.0 K interval. (c) Zone-center temperature dependence of the band associated with defect site Fe^{3+} and q-AFM ($\omega_{q\mathrm{AFM}}$) and q-FM ($\omega_{q\mathrm{FM}}$) magnon modes of $LuFeO_3$ using the 110 K spectrum as normalizing reference.

a consequence of precessing moments under inhomogeneous individual exchange and dampings excluded in the two-site picture. In this regard, it is also worth noting that the ZFC $\omega_{q\mathrm{FM}}$ mode at 14.7 cm^{-1} (Fig. S4 in the Supplemental Material [15], upper panel) has a band profile wide enough that may also be reproduced by two bands as for contemplating the existence of a zero-field extra-weaker intrinsic exchange. This, nonetheless, does not exclude considering the overall behavior of q-AFM- and q-FM-like magnons in $LaFeO_3$ as a suitable standard against the characterization shown in the following subsections for the $RFeO_3$ (R = Pr, Er, Lu) orthoferrites.

B. $PrFeO_3$

Highly correlated non-Jahn-Teller $PrFeO_3$ is a Fe^{3+} high-state-distorted orthorhombic perovskite in which the A-site rare-earth–oxygen distances embrace eight nearest neighbors out of the cubic 12 (Fig. 2), conforming to a sublattice in

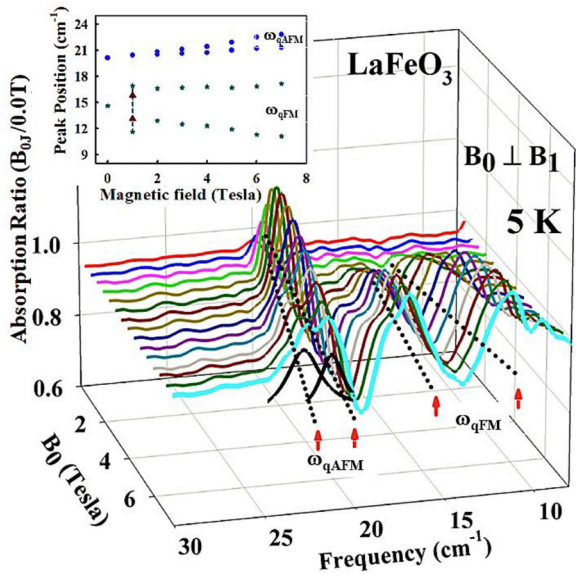

FIG. 4. $LaFeO_3$ quasiantiferromagnetic and quasiferromagnetic spin-wave resonances as a function of the applied magnetic field B_0 at 5 K. Inset: Peak positions of the shown absorptions after Gaussian fits (Fig. S4 in the Supplemental Material [15]).

which the lanthanide $4f^2$ shell has CF $^3H_4$ ground state in which the multiplet CF splits into nine singlets.

This compound, as for $LaFeO_3$, is in the room-temperature Γ_4 (G_x, A_y, F_z) magnetic representation below the Néel temperature $T_N \sim 703$ K [74,75]. It also develops below T_N weak FM along the c axis due to the Fe^{3+} canted moment with angle α (deg.) $= 0.49°$ [69]. On decreasing temperature, a broad inflexion in the reciprocal magnetic susceptibility has been associated with a spontaneous spin reorientation turning, between 201 and 140 K, Γ_4 (G_x, A_y, F_z) into Γ_2 (F_x, C_y, G_z) rotating magnetic moments in the ac plane due to $4f$-$3d$ competing exchanges by Pr^{3+} and Fe^{3+} [21]. However, against this observation, neutron diffraction patterns at 8 K confirm the G_x-type AFM arrangement. It also supports earlier conclusions by which weak Pr-Fe couplings question the possible reorientation phase transition [20].

We will assume that, in our measurements, the Γ_4 (G_x, A_y, F_z) representation holds in the temperature range of our studies.

At low temperatures, we find a distinctive band at ∼16.6 cm^{-1} that becomes sharper and that is also central to two much weaker and broader ones [Fig. 3(b)]. It softens, undergoing an energy downshift with ZFC from 5 to ∼2 K, likely a consequence of exchange couplings that, without an apparent change in the side band profiles, retain the high-temperature magnetic representation Γ_4 (G_x, A_y, F_z). The central feature matches inelastic neutron data at 16 cm^{-1} (2.0 ± 0.1 meV) assigned to the lowest of the $2J+1$ $^3H_4$ ground state level [76]. It has an asymmetric band shape reproduced by an overall Weibull profile due to its coalescing into near degeneracy with the bands at ∼9.9 and ∼25.5 cm^{-1} contributing to the fused profile (Fig. S6 in the Supplemental Material [15]). These last two are assigned to the $\omega_{q\mathrm{AFM}}$ and $\omega_{q\mathrm{FM}}$ modes by association with the resonances found in $LaFeO_3$. The emerging picture is close to what we reported earlier for $PrCrO_3$, where it was possible to deconvolute that main band into three components despite that transition metal anisotropy fields together with the paramagnetic Pr^{3+} moments add random fluctuations in the q-AFM mode, dynamically blurring magnetic oscillations [77]. In $PrFeO_3$, this would prevent well-defined q-AFM x, y out-of-phase and in-phase oscillations along the z axis and q-FM low-frequency

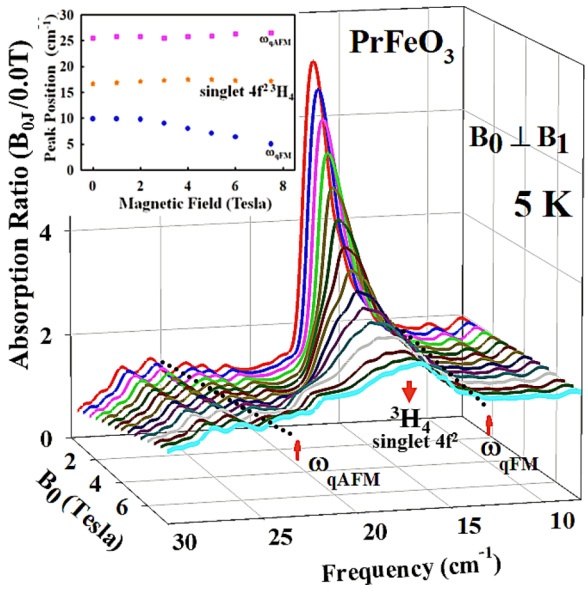

FIG. 5. First excited state of the $Pr^{3+}(4f^2)$ $^3H_4$ manifold and weaker side bands assigned to the $\omega_{q\mathrm{FM}}$ and $\omega_{q\mathrm{AFM}}$ resonances in $PrFeO_3$ as a function of the applied magnetic field B_0 at 5 K. Inset: Peak positions of the shown absorptions after Gaussian and Weibull fits (Fig. S7 in the Supplemental Material [15]).

cones delineated by the FM moment precessing the z axis (Fig. 1).

To have a better picture of the low-energy spin dynamics and possible field-induced $3d$-$4f$ coupling along spin fluctuations, we also applied an external magnetic field. Figure S7 in the Supplemental Material [15] shows that now, and as in $PrCrO_3$ [77], the lowest of the $2J+1$ $^3H_4$ ground state level behaves as expected for a $4f$ even-electron lanthanide in ground crystal singlets being up to 7 T nearly unaffected by the external field [78]. There is, however, an effective weakening, broadening, and merging that may mask unresolved weak field dependences. Consequently, we only have significant departures from linearity in the broad feature assimilated to the $\omega_{q\mathrm{FM}}$ Fe^{3+} resonant mode. In either case, there is no field-induced split degeneracy, as found in $LaFeO_3$, but a field-increase-induced broadening, suggesting that magnon splitting may be screened out due to the Pr^{3+} paramagnetism further disturbing magnetic couplings and anisotropies of the in-phase oscillation ($\omega_{q\mathrm{AFM}}$) and precession ($\omega_{q\mathrm{FM}}$) that in the presence of the ground state dipole transition appear merging all excitations into one highly coupled mixed scenario. The relative clean profile for the ground level at weaker fields becomes a band with much less oscillator strength turning near featureless under 7.5 T at 5 K (Fig. 5). This is a likely consequence, again, of magnetodynamical fields in a mixed scenario in which the local microscopically altered lattice structure may also play a role [79].

C. $LuFeO_3$

The magnetic-dependent features found in $LaFeO_3$ are also expected for orthorhombic $Pbnm$-D_{2h}^{16} $LuFeO_3$ ($T_N \sim 623$ K) [80] since main differences in bulk properties are only introduced by the replacement of La by the also closed electronic shell Lu ($4f^{14}$). Both compounds, $LaFeO_3$ and $LuFeO_3$, share the Γ_4 (G_x, A_y, F_z) magnetic representation at room temperature [24] as well as canted FM here with Fe^{3+} canting angle range $\alpha(\mathrm{deg.}) = 0.80°$ [18] to $0.61°$ [72] relative to the a-oriented sublattice. As Lu^{3+} does not carry a localized magnetic moment, it does not show either magnetic compensation or spin-reorientation effects [81]. We find that, for both compounds, ZFC temperature dependences show profiles that may be assigned to magnons. For $LuFeO_3$, they are at $\omega_{q\mathrm{FM}} \sim 22.4$ cm^{-1} and $\omega_{q\mathrm{AFM}} \sim 26.3$ cm^{-1} [Fig. 2(c)] with an extra third band at $\sim$10.4 cm^{-1}. To understand this last one, it is important to recognize that, in addition to rigid tilting and rotation, the consequence of Lu $4f^14$ smaller ionic radius at the A site is the edge-sharing-inducing ligand distortions that indirectly trigger subtle changes in the octahedral FeO_6 B site. The changes in Fe-O bonding due to this ionic size dependence not only affect the known strong AFM nearest-neighbor Fe-O-Fe exchange interaction but also means a minute but effective local break in the space inversion symmetry allowing Fe^{3+} CF $^6A_1$ multiplet transitions. This slight perturbation at the B sites makes the detection of CF transitions possible and solves the puzzle on the appearance and nature of a third absorption in far-infrared measurements by Aring and Sievers [82]. It also provides a clue about the lattice role in the origin of the ferroelectric loop in the magnetic ordered phase below $\sim T_N$ [83].

The effect introduced by lattice distortions due to smaller lanthanides in $RFeO_3$ has been recognized by phonon Raman scattering measurements [62,84], and it is most distinctive in changes in far-infrared reflectivity when $LaFeO_3$ is compared against $LuFeO_3$ (Figs. S12–S15 in the Supplemental Material [15]). Better defined bands, as for stretching modes $\sim$600 cm^{-1}, and the need for extra oscillators in fits (Tables SI–SIV in the Supplemental Material [15]) suggest minute energy differences translated into smaller ion displacements beyond most of today's x-ray diffraction resolution, and it is at the root of identifying ferroelectric spontaneous polarization in orthorhombic $LuFeO_3$ [85]. It is also close to arguments on lattice strains as its possible origin in $RFeO_3$ thin films making plausible a $Pbn2_1$ space group assignment rather than $Pbnm$ [86], all compounding with the role played by the oxygen electronic polarizability in a ferroelectric phase transition [87]. The oxygen anisotropic volume-dependent nonlinear polarizability, which in ABO_3 introduces a dynamic covalent enhancing in the oxygen p hybridization with iron d states [88], allows a closer unified picture for ferroelectricity beyond introducing foreign antisymmetric coupling of two nonequivalent spin pairs [89]. As has been stressed many times, most ferroelectrics are oxides in which displacive and order/disorder dynamics coexist [90].

Here, Fe^{3+} CF ground level transitions [91] for low-level doped B sites in II–VI compounds are double degenerate and optically active in the lower terahertz portion of the spectra. They have been associated with transitions of the Fe^{3+} $^6A_1$ multiplet in an embedded cage in the α-Al_2O_3 hematite-corundum lattice [92–94] when studying population inversion in Fe^{3+}-doped sapphire [95–97]. We associate our local distortion at B sites with these impurity-induced regimes in which the cubic pure symmetry turns into nearly O_h at distorted sites following the known concurrent structural se-

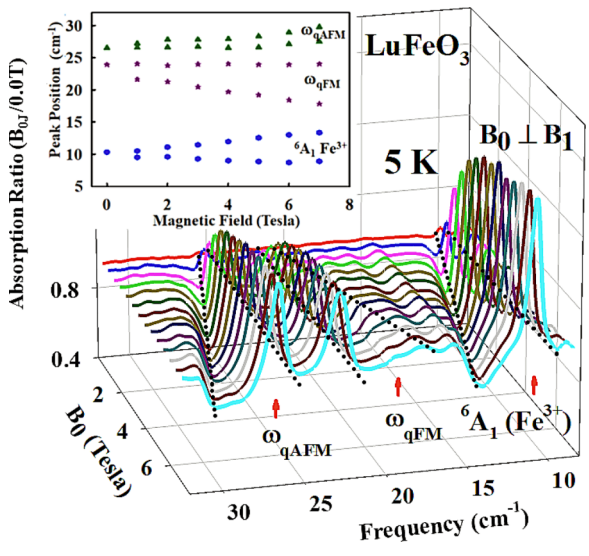

FIG. 6. Zone-center Fe^{3+} ($^6A_1$) crystal-field transition and quasiantiferromagnetic $\omega_{q\mathrm{AFM}}$ and quasiferromagnetic $\omega_{q\mathrm{FM}}$ magnon modes of $LuFeO_3$ as a function of the applied magnetic field B_0 at 5 K. Inset: Peak positions of the shown absorptions after Gaussian and Weibull fits (Fig. S9 in the Supplemental Material [15]).

quence cubic ($CaTiO_3$)-orthorhombic ($RFeO_3$)-rhombohedral (α-Fe_2O_3) [7].

Then the absorption band at $\sim 10\ \mathrm{cm}^{-1}$, Fig. 3(c), and its linear Zeeman branching (Figs. 6 and S8 in the Supplemental Material [15]) are interpreted as from the sextet Fe^{3+} $3d^5$ ($^6S_{5/2}$) in the octahedral CF under a subtle structural distortion [97]. The Fe^{3+} line in $LuFeO_3$ would be the highest Kramers' degenerate level of the three expected to split linearly [93–95]. It accounts for electron-electron repulsion, spin-orbit interaction, and CF potentials [46,98–100].

The energy splitting under external magnetic fields allows us to estimate the g factor using the linear relation:

$$\Delta E = \mu_{\mathrm{B}} g B_0, \tag{5}$$

which holds in the lower-field regime. Here, ΔE is the energy-level Zeeman split shown in Fig. 6 (inset), μ_{B} denotes the Bohr magneton ($\mu_{\mathrm{B}} = 5.788 \times 10^{-5}$ eV/T); g is a dimensionless constant, and B_0 the applied external magnetic field [101]. Our data at 5 K yield $g_{\mathrm{net}} = 1.986$ that, taking it as the result from $\sim$4 near-inequivalent iron sites, coincides within the experimental error with $g_e = 2.0023$ for the free electron. It is the approximate value expected for high-spin d^5 configuration as in transition metals like Fe^{3+}, meaning a very small orbital contribution to the magnetic moment (quenched orbital momentum) with negligible spin-orbit coupling.

The lattice change may be also considered an intermediate step before further departing toward consolidating the hexagonal noncentrosymmetric nonperovskite arrangement. This is a metastable hexagonal structural configuration described by the polar $P63cm$ space group, as in H-$LuFeO_3$, where a trivalent transition metal ion occupies a trigonal bipyramidal site (RO_5) [102,103], rendering the view that low-level A-site substitutions in ABO_3 compounds are functional to weak ferroelectricity [104].

As noted, at slightly higher frequencies than the Fe^{3+} ground transition the two-zone center resonant magnon modes, $\omega_{q\mathrm{FM}}$ and $\omega_{q\mathrm{AFM}}$, are found in zero field cooled runs at $\sim 22.4\ \mathrm{cm}^{-1}$ and $\sim 26.3\ \mathrm{cm}^{-1}$ respectively. The peak positions exhibit a behavior analogous to those in $LaFeO_3$ and are align with an earlier peak quotation by Aring and Sievers [82]. However, in $LuFeO_3$ both resonances under applied fields (depicted in the peripheral insets in Fig. S9 in the Supplemental Material [15]) seem linked by a strong "bridge" that it is only reproduced in fits by introducing an extra background band with distinctive increasing asymmetry. They evenly diverge out the center frame under increasing fields. Herrman [24] pointed out that when considering the four Fe^{3+} magnetic sites, rather than the two sublattice model, it is necessary to take into account not only the so called plain "overt" canting but also a hidden canting mechanism producing no net magnetization. It was found that this last mechanism is particularly significant for the case when the antisymmetric exchange is smaller than the anisotropy energy ($A \gg D$), a case suggested by our $RFeO_3$ (R = rare earth) measurements. We may then conjecture that the optical activity of the bridging excitation at frequencies between the FM and AFM modes stems from an unresolved constituent of hidden canting inducing coupling between exchange and magnon resonances. The exchange resonances by themselves are expected to be optically inactive in antiferromagnetics [24].

We also find a quasi-undulating pattern at $\sim 15\ \mathrm{cm}^{-1}$ (see Fig. S9 in the Supplemental Material [15]. This pattern consists of four emerging very weak maxima indicated by the red arrow in the upper-left 1T inset. At these intermediate frequencies, where the Fe^{3+} branching intersects with the diverging q-FM magnon, (as also shown in Fig. 6), zooming on the $15\ \mathrm{cm}^{-1}$ to $20\ \mathrm{cm}^{-1}$ window allows to deconvolute each weak peak by partially superimposing two broad Gaussians. For simplicity, the remaining three are omitted. We interpret the four individual peaks as arising from inequivalent magnetic sites that ought to be taken into account if considering inequivalent four Fe^{3+} magnetic sites rather than the two sublattices of the present working hypothesis [24]. These weak features also appear with similar frequency spread on the mode higher-frequency branching of $\omega_{q\mathrm{AFM}}$ (see also Fig. S10 in the Supplemental Material [15]) corroborating that both resonances, $\omega_{q\mathrm{AFM}}$ and $\omega_{q\mathrm{FM}}$, are indeed intertwined in a collective complex trend. This collective behavior, along with the effects of polycrystallinity that blurs individual phase motion, may be then associated to the rare earth-induced A site lattice perturbations. These perturbations, at the root of spin canting single-ion anisotropy [18], is the cause the optical activity of the Fe^{3+} ion in disturbed lattice sites as addressed in previous and following paragraphs.

D. $ErFeO_3$

Here, $ErFeO_3$ ($T_{\mathrm{N}} \sim 633$ K) [31,63] orthorhombic $Pbnm$-D_{2h}^{16} is perhaps one of the most studied compounds of the ferrite family [105]. Starting at $\sim$220 K and on cooling [106], Er^{3+} moments start forcing the prevailing magnetic-oriented iron moments in the Γ_4 (G_x, F_z) representation to rotate 90° into the F_2 (G_z, F_x) a-axis alignment in an interval from $T_1 = 87$ K (90 K) to $T_2 = 96.6$ K

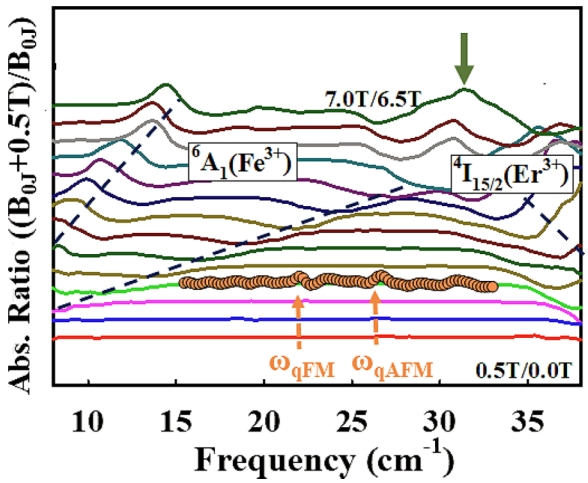

FIG. 7. $ErFeO_3$ sequential absorption ratios $(B_{0j} + 0.5T)/B_{0j}$, where B_{0j} is the applied field at the jth incremental step, projecting field-dependent Zeeman splits of Fe^{3+} ($^6A_1$) and Er^{3+} ($^4I_{15/2}$) and resonant magnon mode (dashed arrows) at the compensation temperature ∼40 K. Note that both resonances are inside a triangle defined by the highest Fe^{3+} ($^6A_1$) and lowest Er^{3+} ($^4I_{15/2}$) branch exchange converging at ∼5 T. The solid arrow points to the anomaly associated with paramagnetic Er^{3+}.

(103 K) [107–112]. This mostly magnetic displacive phase transition, in which strong spin-lattice coupling has also been reported, is common to canted FM in all partially filled rare-earth f-odd shell compounds [8,30,31,99,102].

We studied in this Γ_2 (G_z, F_x) phase the Fe^{3+} ($^6A_1$) and Er^{3+} ($^4I_{15/2}$) manifolds as well as the two spin resonances. As shown in the mapping of an incremental field plot, Fig. 7, the Fe^{3+} ($^6A_1$) transition, extrapolated in our detection limit to ∼4 cm^{-1}, undergoes a linear Zeeman split in a perturbed A site close to behaving as discussed in the section for $LuFeO_3$. However, unlike the symmetric profile in $LuFeO_3$ (Fig. 6), it is now biased toward higher energies due to a drift associated with the Er^{3+}–Fe^{3+} magnetic exchange.

Figure 8(a) shows that, on cooling, the intensity of the q-AFM resonance increases continuously below the reorientation temperature T_{RS} peaking at ∼5 K to then turning into a sharp decrease as $ErFeO_3$ gets closer to the Γ_1 (A_x, G_y, C_z) phase. In this phase, after softening, it merges with the much weaker hardening FM mode (ω_{qFM}). This results in a single much broader feature characteristic of the Γ_1 phase as the Fe^{3+} spins undergo a gradual G_z-to-G_y rotation due to Er^{3+} exchange coupling, leading to cooperative AFM for Er^{3+} below $T_N(Er) \sim 4.5$ K [Figs. 8(a) and 8(b)]. This behavior is like what has been reported for $ErCrO_3$ in the same temperature range [77]. The sharp decrease of the ω_{qAFM} mode intensity signals the onset of the $G_{xy}F_x$ mixed spin arrangement [113] at the time that the corresponding magnetic structure turns into fully C_z AFM oriented for Er^{3+} and magnetic $C_yG_zF_x$ for Fe^{3+} [114,115] in a potential low-temperature monoclinic space group $P21/m$.

It is also worth underlining that, in our studies, we do not observe an anomaly, electric-dipole related, that might be assigned at the lowest temperatures to an electromagnon even upon applying moderate external magnetic field, as was reported in nominally isomorphic $TbFeO_3$ [116] and $DyFeO_3$ [117]. In an electromagnon, rare-earth magnetic moments would align with the field (either from perturbating Fe^{3+} or external), causing a change in the electric polarization that would possibly be detected as extra absorption in terahertz–far-infrared measurements.

The q-FM and q-AFM resonances in $ErFeO_3$ at $\omega_{qFM} \sim 21.5$ cm^{-1} and $\omega_{qAFM} \sim 31.5$ cm^{-1} have an equally weak field dependence up to the compensation temperature T_{CMP} [113]. This is the temperature at which the AFM exchange interaction of paramagnetic Er^{3+} moment equals the near-constant moment of Fe^{3+} spins, meaning a net polarization of the Er^{3+} spins antiparallel to the canted Fe^{3+} [118,119]. That

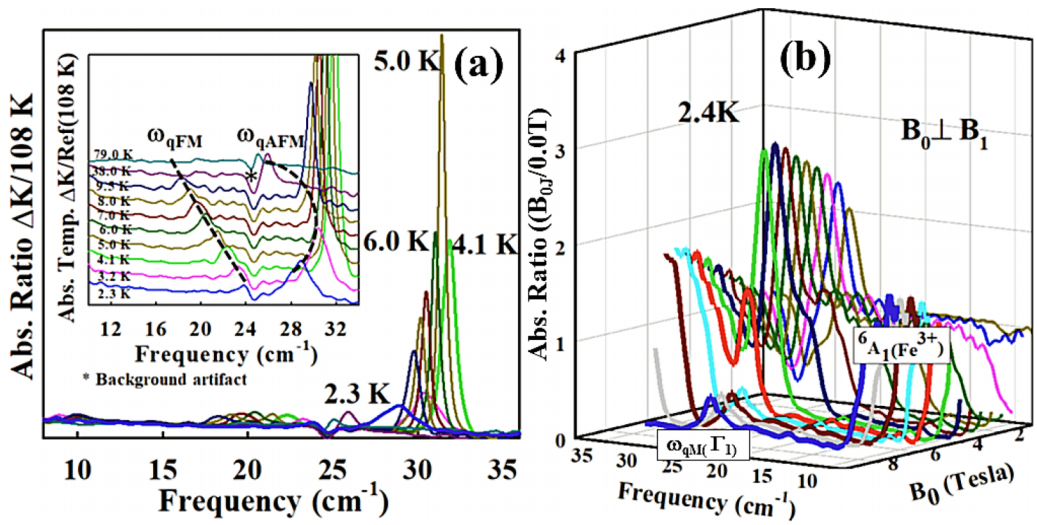

FIG. 8. (a) $ErFeO_3$ temperature dependence of the resonance ratios using the 108 K spectrum as reference. Inset: The same data vertically displaced showing the convergence of both magnons toward the onset of the lower-temperature Γ_1 representation. (b) Applied field-dependent $ErFeO_3$ magnon absorption in the zero-field cooled (ZFC) Γ_1 (A_x, G_y, C_z) phase, at 2.4 K, below and at the interfering Fe^{3+} Zeeman field split.

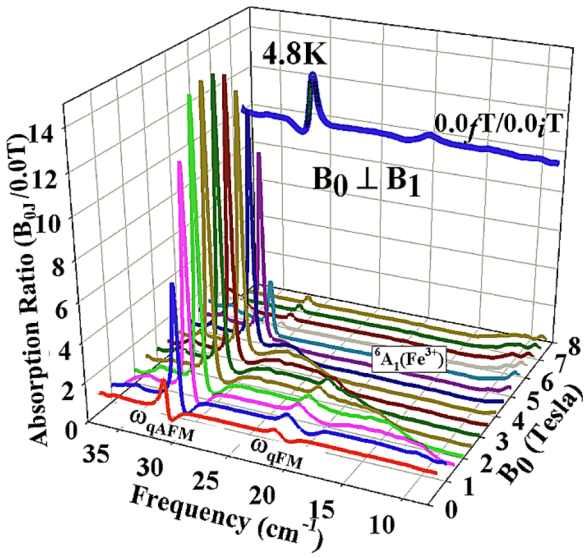

FIG. 9. $ErFeO_3$ absorption ratios ($B_{0j}/0.0T$), where B_{0j} is the applied field at the jth incremental step, for the terahertz excitations and exchange-biased zone-center Fe^{3+} ($^6A_1$) Zeeman split at 5 K. The full line in the back panel shows memory effects brought up by calculating the ratio of spectra of measurements done at the initial and end run at zero field and 5 K.

is, the negative exchange interaction of the iron and erbium yields a total spontaneous moment written as

$$M = M_0 + \varkappa_R H_0, \tag{6}$$

where M_0 is the FM moment,$\varkappa_R$ the paramagnetic rare-earth susceptibility, and H_0 the exchange field at the rare earth by the irons. With negative exchange interaction, the rare-earth-induced magnetic moment decreases, and so the total magnetic moment diminishes up to vanishing at T_{CMP} [120]. A vanishing point also remains upon applying an external magnetic field such that, at temperatures above it, the canted FM is directed along the field.

Here, $ErFeO_3$ field-dependent-induced absorptions from terahertz resonances and Zeeman splits are shown using the ZFC spectrum at 5 K as a reference in Fig. 9. As in their temperature dependence, the induced change at the q-AFM resonance undergoes a huge enhancement, while the rather weak q-FM mode behaves accordingly to the previous cases. However, different from what we found for the other compounds, they do not diverge split upon applying up to 7 T. It appears as if their divergency is compensated by the Fe^{3+}-Er^{3+} exchange yielding a very narrow picture that, unsolved at our working resolution, increases in intensity, assuming superposing two Gaussians.

Zero-field ratios calculated using the spectra taken for the initial and after the 7 T run yield extra absorptions at both magnon frequencies, bringing up the delicate nature of the exchange on these modes. Interpreted as a memory effect, this behavior may also help to explain the origin of the broad and intriguing extra line reported by Mikhaylovskiy *et al.* [121]. Our spectra show that, at zero field, the Fe^{3+} unfolded multiplet and zone-center magnons are separated by at least 15 cm^{-1}, thus ruling out a zone-center interference as a possible explanation. Rather, the unexplained extra band at 11.7 cm^{-1} (0.35 THz) shouldering the FM mode might have been created by a laser-induced distortion locally changing the effective temperature within the dynamics of the resonant mode.

Alongside the temperature-dependent–field-dependent changes of the magnetic resonances, the overall picture for the Fe^{3+} and Er^{3+} multiplet transitions remains essentially unaltered (Fig. S11 in the Supplemental Material [15]). We note, however, that bands of the Zeeman Fe^{3+} lower-energy branch associated with intensity increments, at increasing field ratios, correspond to a shallow response in the branch facing the Er^{3+} ($^4I_{15/2}$) Zeeman split at higher frequency. Only when ratios for this last one are calculated with decreasing fields, we retrieve meaningful Gaussian profiles (blue traces in Figs. 10 and S11 in the Supplemental Material [15]), suggesting depopulated levels due to Er^{3+} exchange. The applied field selectively disrupts the known symmetric part of the exchange energy between the two Fe^{3+} magnetic sublattices S_i and S_j and thus the zero-field superexchange involving nearest-neighbor Fe+ ions via the intermediate O^{-2} ion. In zero-field superexchange, one spin-up electron virtually hops to oxygen, forming an up-down pair, and back to the same spin orientation [122]. We find that this mechanism is particularly sensitive to the paramagnetic Er^{3+} lowest Zeeman branch when the higher Fe^{3+} and lower Er^{3+} branches meet at $T_{CMP} \sim 40$ K at ~ 30 cm^{-1} and ~ 5 T (solid arrow in Fig. 5). In this scenario, and in contrast with the clean picture suggested by the $LuFeO_3$ analysis, the calculation of the g factor now reflects increasing couplings and anisotropies induced by the ligand field in what would imply a net effective result. Choosing energy levels at intermediate fields from the skew Zeeman split shown in Fig. 10(a) and replacing B_0 by $B_{\text{eff}} = (B_0 + L_{\text{ocal}})$ and g by g_{eff} in Eq. (5) [102], we found $L_{\text{ocal}} \sim 1.08$ T that in turn results in a ballpark $g_{\text{eff}} \sim 10.0 \pm 0.5$.

While there is Fe^{3+} ($^6A_1$) population inversion at all temperatures, in the Er^{3+} branch, it is only associated with paramagnetic Er^{3+} random dipoles. In $ErFeO_3$, the field-dependent extra absorption at 40 K of ~ 30 cm^{-1} and ~ 5 T diminishes as Er^{3+} gets closer to its ordered AFM phase, where branching becomes near field independent. At 5 K, the induced change becomes undetectable, and at 2.4 K, it has totally disappeared, allowing undistorted Gaussian profiles in the Fe^{3+} ($^6A_1$) higher-frequency branch [Figs. 10(b) and S11 in the Supplemental Material [15]).

E. Er^{3+} multiplet and phonon field dependences

To get a full view of the temperature field dependence of the Er^{3+} ($^4I_{15/2}$) multiplet, it is necessary to run far-infrared spectra. In this range, the near-normal reflectivity of $ErFeO_3$ at 5 K, Fig. S13 in the Supplemental Material [15], is dominated by phonon profiles that may be broadly grouped into a lower-frequency region centered at ~ 200 cm^{-1} for lattice vibrations in which the rare earth moves against the FeO_6 sublattice, a second one centered at ~ 350 cm^{-1} that it is characterized by Fe scissor and stretching modes as well as octahedral librations, and a third one for oxygen breathing-stretching modes at ~ 600 cm^{-1}. When this reflectivity is matched to the absorption ratio of 1 T against 0 T spectra,

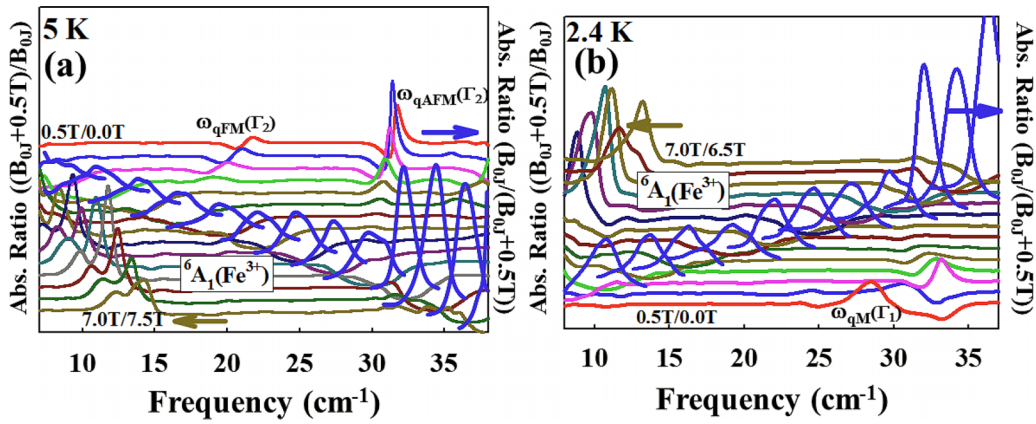

FIG. 10. (a) Applied field-dependent Zeeman split of Fe^{3+} ($^6A_1$) and Γ_2 magnons. Left axis: Sequential absorption ratios $(B_{0j}+0.5T)/B_{0j}$, where B_{0j} is the applied field at the jth incremental step at 5 K. Right axis: Sequential absorption ratios $B_{0j}/(B_{0j}+0.5T)$ calculated decreasing fields at 5 K. (b) Applied field-dependent Zeeman split of Fe^{3+} ($^6A_1$). Left axis: Sequential absorption ratios $(B_{0j}+0.5T)/B_{0j}$, where B_{0j} is the applied field at the jth incremental step at 2.4 K. Right axis: Sequential absorption ratios $B_{0j}/(B_{0j}+0.5T)$ calculated decreasing fields at 2.4 K. The measured profile for the Γ_1 magnon is shown centered at $\sim$28.5 cm^{-1}.

Fig. 11(a), it is straight forward to locate the three Er^{3+} ($4f^{11}$) Kramers' ($^4I_{15/2}$) doublets, as their magnetic signature appears at 49.5 cm^{-1} (6.14 meV), 110.5 cm^{-1} (13.7 meV), and 167.3 cm^{-1} (20.74 meV). They are in agreement with recent inelastic neutron scattering measurements [115,120] and earlier estimates [123].

Just 0.5 T is enough to lift the Er^{3+} Kramers' degeneracy by $\sim$5 cm^{-1} (0.62 meV) into two weaker bands. At temperatures below the compensation point $T_{CMP} \sim 40$ K, and increasing the fields, Fig. 12, they turn into strong asymmetric Zeeman splits correlated with the Fe^{3+} branching at lower frequencies. While this asymmetric picture is seen for the three transitions, it is particularly clear for the third level at 167.3 cm^{-1} being symmetric above T_{CMP} to then have a field-insensitive lower-frequency branch as it becomes associated with the Fe^{3+} exchange at and below T_{CMP} (Fig. S16 in the Supplemental Material [15]).

Here, Er^{3+} levels at 110.5 and 167.3 cm^{-1} fall at known reflectivity phonon frequencies for vibrational modes involving rare-earth displacements and, least for one case, seems to also be related to an A_g phonon in Raman spectra that for $LaFeO_3$ is at 84.5 cm^{-1} [50]. Figure 11(a) also shows a dotted line across a continuous envelope in the field-induced absorption of the 1 T/ 0 T ratio coinciding with the region of external lattice vibrations. It suggests localized charge delocalization for the frequencies where phonons are found interacting with the CF levels and thus spins. This is at the root of the so-called phonomagnetism, where phonons induce magnetism by light

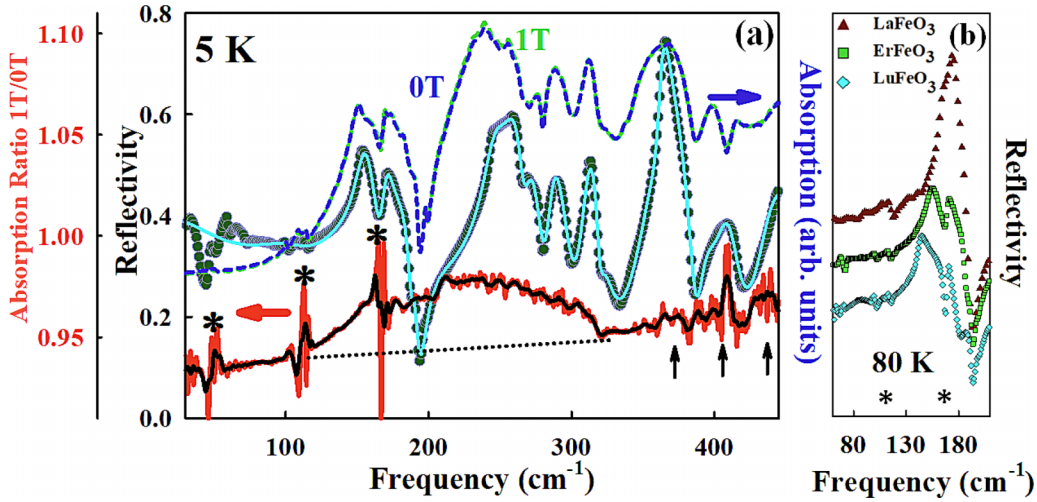

FIG. 11. $ErFeO_3$ far-infrared absorption, reflectivity, and 1.0 T/0.0 T zero-field cooled (ZFC) absorption ratio at 5 K [15]. (a) Dashed lines: $ErFeO_3$ powder embedded polyethylene pellet absorption spectra at 0 and 1 T; circle and full line: polycrystal reflectivity spectra and multioscillator fit, respectively; full lines: 1.0 T/0.0 T ZFC absorption ratio; asterisks: peak position for the 49.5 cm^{-1} (6.14 meV), 110.5 cm^{-1} (13.7 meV), and 167.3 cm^{-1} (20.74 meV) transitions of the Er^{3+} ($^4I_{15/2}$) manifold. (b) Vertically displaced reflectivity of $RFeO_3$ (R = La, triangle; Er, square; Lu, diamond), showing relative changes in the R^{3+}-O vibrational profiles induced by the change in the lanthanide size at 80 K. Asterisks: ZCF transitions of the Er^{3+} ($^4I_{15/2}$) manifold associated to lattice phonons at the respective frequencies.

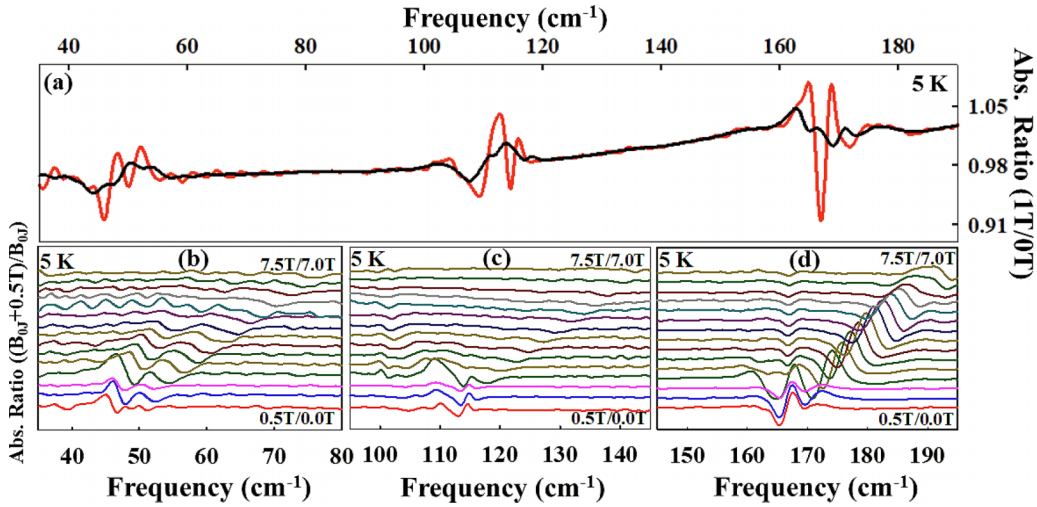

FIG. 12. (a) Ratio of $ErFeO_3$ powder embedded polyethylene pellet 5 K spectra at 1 and 0 T absorptions peaking at the 49.5 cm^{-1} (6.14 meV), 110.5 cm^{-1} (13.7 meV), and 167.3 cm^{-1} (20.74 meV) transitions of the Er^{3+} ($^4I_{15/2}$) manifold. (b)–(d) Vertically offset Zeeman split sequential absorption ratios $(B_{0j} + 0.5T)/B_{0j}$, where B_{0j} is the applied field at the jth incremental step, of the Er^{3+} ($^4I_{15/2}$) levels showing the bias induced by the Fe^{3+} exchange on the lower-frequency branch (see also Fig. S16 in the Supplemental Material [15]).

excited lattice distortion, modifying the rare-earth transition exchange interaction. It has been recently shown that non-thermal resonance driven by light phonons may be used to manipulate magnetic states in exchange interactions between rare-earth orbitals and transition metal spins switching AFM and weakly FM spin orders [124].

Next, at increasing frequencies, there are three individual field enhancements centered at $\sim$400 cm^{-1}, the frequency for Fe^{3+} torsional vibrations [vertical arrows in Fig. 11(a)]. Each phonon corresponds to a field-induced absorption that becomes stronger at frequencies closer to the respective LO mode associated with the reflectivity TO-LO reststrahlen split. Nonlinear vibrational modes are also found to drive rotations and displacements, mimicking the application of a magnetic field, yielding spin precession as a tool for stimulation of optomagnetic phenomena [125].

Also shown in Fig. S13 in the Supplemental Material [15], under 1 T, we do not find a magnetic response for breathing stretching modes centered at $\sim$600 cm^{-1} where only oxygens move. Field dependences are only detected for vibrations involving moving magnetic ions, in our case Er^{3+} and Fe^{3+}, fulfilling the basic premise in TO-LO magnetoelectrics by which ion displacements couple electric and magnetic contributions appearing in the macroscopic field [9]. This contrasts with dielectric insulators where the macroscopic field linked to a LO mode is only associated with long-range electric fields as restoring force due to Coulomb interactions and by which LO frequency is a minimum over its reststrahlen [10].

V. CONCLUSIONS

Summarizing, we studied low-temperature–low-energy absorptions of $LaFeO_3$ AFM and FM magnons at $\omega_{q\mathrm{FM}} \sim$ 26.7 cm^{-1} and $\omega_{q\mathrm{AFM}} \sim$ 31.4 cm^{-1} in the Γ_4 (G_x, A_y, F_z) representation. We found that their degeneracy is lifted about linearly by an applied field up to 7 T. In isomorphic $LuFeO_3$, in addition to these two spin modes, now peaking at $\omega_{q\mathrm{FM}} \sim$ 22.4 cm^{-1} and $\omega_{q\mathrm{AMF}} \sim$ 26.3 cm^{-1}, there is a Fe^{3+} CF $^6A_1$ transition at $\sim$10.4 cm^{-1} whose activity is tied to ligand distortions induced by the Lu^{3+} $4f^{14}$ smaller ionic radius. This A-site deformation triggers subtle lattice changes at the perovskite B site and allows a linear Zeeman split up to 7 T. It is also found in $ErFeO_3$ [Kramers' $4f^{11}$ Er^{3+}; Γ_2 (F_x, C_y, G_z) $< T_{\mathrm{SR}} \sim$ 93 K], where now the Fe^{3+} Zeeman branching is strongly biased toward higher energies due to $3d$-$4f$ exchange. Within our 0.5 cm^{-1} working resolution at 5 K, and in contrast with magnons in $RFeO_3$ (R = La, Lu), there is no field-induced split, but a low-temperature 13-fold increase in the intensity of the resonance AFM/FM mode ratio. It is also remarkable that the CF matching population balances between Fe^{3+} higher and Er^{3+} lower Zeeman-split branches.

Here, Er^{3+} ($^4I_{15/2}$) transition energies from the ground multiplet at 110.5 and 167.3 cm^{-1} coincide with external lattice mode frequencies, suggesting strong CF-phonon couplings in a scenario for lattice-driven spin-phonon interactions. Absorption spectra ratios under mild external fields reveal a magnetic-dependent local quasicontinuum in the Er-O vibrational region and enhancement in LO mode macroscopic fields associated with Fe^{3+} torsional modes, i.e., field dependences are only detected for vibrations involving moving magnetic ions.

AFM and FM resonances turn in $PrFeO_3$ much broader when non-Kramers' Pr^{3+}, with two unpaired $4f^2$ electrons, introduces ligand changes at the A site, leading the $\omega_{q\mathrm{AFM}}$ mode and the lowest Pr^{3+} CF transition into near degeneracy. This and the $\omega_{q\mathrm{FM}}$ merge at 7 T into a single broad mostly unresolved feature.

We conclude that low-energy excitations in $RFeO_3$ (R = rare earth) strongly depend on the lanthanide ionic size thus indivisibly tied to the mechanism associated with the origin of canted FM. Minute lattice displacements in the perovskite basic BO_6 and AO_{12} building blocks also underlie the fact that the ferroelectric instabilities might already be present above T_c at sites with thermal distribution of the ionic motion. Peaking at actual centrosymmetric sites may really be due to

some multiwell configuration, as most ferroelectrics appear to be in the middle ground represented by shallow double wells and anharmonic rough single wells [126]. This argument motivates the possibility of assigning noncentrosymmetry to those distorted perovskites with smaller rare-earth ionic radius as for the $Pbn2_1$ space group, i.e., with Fe^{3+} not at the center of inversion in a rigid ion approximation. Then it is necessary to also consider the hybridization between oxygen p and transition metal d electrons. As a feature in driving the ferroelectric instability, it will dynamically enhance the oxygen volume-dependent electronic polarizability that it is tied to the emergence of the weak spontaneous polarization within the framework of most known ferroelectric oxides [90,126].

ACKNOWLEDGMENTS

The authors are pleased to acknowledge the enlightening insights and full support at the terahertz beamline by K. Holldack [Department Optics & Beamlines, Helmholtz-Zentrum für Materialien und Energie GmbH (HZB), D-12489] during the development of this paper. N.E.M. is indebted to BESSY II at the Helmholtz-Zentrum Berlin für Materialien und Energie for beamtime allocation under Proposals No. 201–09204-ST, No. 202–09707-ST, No. 212–10296-ST, No. 221–10915-ST, No. 221–10941-ST, No. 222–11422-ST, and No. 222–11426-ST and for financial assistance supported by the project CALIPSO plus under Grant Agreement No. 730872 from the European Union Framework Program for Research and Innovation HORIZON 2020. He also thanks the laboratory on Conditions Extrêmes et Matériaux: Haute Température et Irradiation—UPR3079 CNRS (C.E.M.H.T.I.) in Orléans and the Groupement de Recherche Matériaux Microélectronique Acoustique Nanotechnologies (GREMAN-UMR7347 CNRS), Université de Tours, Tours, for sharing expertise on research and financial support performing far-infrared reflectivity measurements. J.A.A. acknowledges ILL-Grenoble for the allowed neutron time and the financial support of the Spanish Ministry for Science and Innovation (No. MCIN/AEI/10.13039/501100011033) for granting Project No. PID2021-122477OB-I00-R.

[1] M. Fiebig, T. Lottermoser, D. Meier, and M. Trassin, The evolution of multiferroics, Nat. Rev. Mater **1**, 16046 (2016).
[2] N. A. Spaldin and M. Fiebig, The renaissance of magnetoelectric multiferroics, Science **309**, 391 (2005).
[3] N. D. Todorov, M. V. Abrashev, and V. G. Ivanov, Frequency dependence of the quasi-soft Raman-active modes in rotationally distorted $R^{3+}B^{3+}O_3$ perovskites (R^{3+} = rare earth, B^{3+} = Al, Sc, Ti, V, Cr, Mn, Fe, Co, Ni, Ga), J. Phys.: Condens. Matter **24**, 175404 (2012).
[4] H. Forestier and G. Guiot-Guillain, Une nouvelle série de corps ferromagnetiques: Les ferrites de terres rare, C. R. Acad. Sci. **230**, 1844 (1950).
[5] D. Treves, Studies on orthoferrites at the Weizmann Institute of Science, J. Appl. Phys. **36**, 1033 (1965).
[6] R. L. White, Review of recent work on the magnetic and spectroscopic properties of the rare-earth, J. Appl. Phys. **40**, 1061 (1969).
[7] Magment GmbH, Germany; https://www.magment.co/.
[8] R. Resta, Lyddane-Sachs-Teller Relationship in Linear Magnetoelectrics, Phys. Rev. Lett. **106**, 047202 (2011).
[9] P. Yu and M. Cardona, Vibrational properties of semiconductors, and electron phonon interaction, *Fundamentals of Semiconductors*, 2nd ed. (Springer-Verlag, Berlin, 1999).
[10] S. M. Shapiro, J. D. Axe, and J. P. Remeika, Neutron-scattering studies of spin waves in rare-earth orthoferrites, Phys. Rev. B **10**, 2014 (1974).
[11] M. Marezio, J. P. Remeika, and P. D. Dernier, The crystal chemistry of the rare earth orthoferrites, Acta Cryst. B **26**, 2008 (1970).
[12] D. J. Lam, B. W. Veal, and D. E. Ellis, Electronic structure of lanthanum perovskites with 3*d* transition elements, Phys. Rev. B **22**, 5730 (1980).
[13] E. F. Bertaut, in *Magnetism: A Treatise on Modern Theory and Materials*, edited by G. T. Rado and H. Suhl (Academic Press, New York, 1963), Vol. 3, p. 149.
[14] F. Bertaut and F. Forrat, Structure des Ferrites Ferrimagnétiques des Terres Rares, C.R. Acad. Sci. **242**, 382 (1956).
[15] See Supplemental Material at http://link.aps.org/supplemental/10.1103/PhysRevB.108.115116 for information on sample preparation, x-ray diffractograms, and magnetic characterization; layout of the terahertz beamline at BESSY II; $RFeO_3$ (R = La, Er, Lu) far-infrared data and multioscillator fits; temperature dependence of Fe^{3+} ($^6A_1$) and Er^{3+} ($^4I_{15/2}$) CF Zeeman and quasimagnons from 110 to 2.4 K in $ErFeO_3$; $ErFeO_3$ far-infrared Er^{3+} ($^4I_{15/2}$) Zeeman multiplet biased due to Fe^{3+} ($^6A_1$) exchange from 75 to 2.3 K. The Supplemental Material also contains Refs. [52–55] therein.
[16] T. Yamaguchi, Theory of spin reorientation in rare-earth orthochromites and orthoferrites, J. Phys. Chem. Solids **35**, 479 (1974).
[17] A. Moskvin, Dzyalonshinkii-Moriya coupling in 3*d* insulators, Condens. Matter. **4**, 84 (2019).
[18] J.-S. Zhou, L. G. Marshall, Z.-Y. Li, X. Li, and J.-M. He, Weak ferromagnetism in perovskite oxides, Phys. Rev. B **102**, 104420 (2020).
[19] H. Homer and C. M. Varma, Nature of Spin-Reorientation Transitions, Phys. Rev. Lett. **20**, 845 (1968).
[20] P. Pataud and J. Sivardière, Chaleurs Spécifiques a Basse Température de Quelques Orthoferrites et Orthochromites de Terres Rares, J. De Physique **31**, 1017 (1976).
[21] Z. Zhou, L. Guo, H. Yang, Q. Liu, and F. Ye, Hydrothermal synthesis and magnetic properties of multiferroic rare-earth orthoferrites, J. Alloys Compd. **583**, 21 (2014).
[22] K. P. Belov, A. K. Zvezdin, and A. M. Kadomtseva, Rare-earth orthoferrites, symmetry and non-Heisenberg exchange, *Soviet Scientific Reviews, Section A. Physics Reviews* (Harwood Academic Publishers, 1987), pp. 117–222.
[23] C. H. Tsang, R. L. White, and R. M. White, Spin wave damping of domain walls in $YFeO_3$, J. Appl. Phys. **49**, 6063 (1978).
[24] G. F. Herrmann, Magnetic resonances and susceptibility in orthoferrites, Phys. Rev. **133**, A1334 (1964).
[25] G. F. Herrmann, Resonance and high frequency susceptibility in canted antiferromagnetic substances, J. Phys. Chem. Solids **24**, 597 (1963).

[26] R. M. White, R. J. Nemanich, and C. Herring, Light scattering from magnetic excitations in orthoferrites, Phys. Rev. B **25**, 1822 (1982).

[27] C. Kittel, Theory of antiferromagnetic resonance, Phys. Rev. **82**, 565 (1951).

[28] T. Nagamiya, Theory of antiferromagnetism and antiferromagnetic resonance absorption, Prog. Theor. Phys. **6**, 342 (1951).

[29] F. Keffer and C. Kittel, Theory of antiferromagnetic resonances, Phys. Rev. **85**, 329 (1952).

[30] N. Koshizuka and S. Ushioda, Inelastic-light-scattering study of magnon softening in $ErFeO_3$, Phys. Rev. B **22**, 5394 (1980).

[31] N. Koshizuka and K. Hayashi, Raman scattering from magnon excitations in $RFeO_3$, J. Phys. Soc. Jpn. **57**, 4418 (1988).

[32] G. V. Koslov, S. P. Lebedev, A. A. Mukhr, A. S. Prokhorov, and L. V. Fedorov, Submillimeter backward-wave oscillator spectroscopy of the rare-earth orthoferrites, IEEE Trans. on Magnetics **29**, 3443 (1993).

[33] R. V. Mikhaylovskiy, T. J. Huisman, A. I. Popov, A. K. Zvezdin, Th. Rasing, R. V. Pisarev, and A. V. Kimel, Terahertz magnetization dynamics induced by femtosecond resonant pumping of Dy^{3+} subsystem in the multisublattice antiferromagnet $DyFeO_3$, Phys. Rev. B **92**, 094437 (2015).

[34] E. Constable, D. L. Cortie, J. Horvat, R. A. Lewis, Z. Cheng, G. Deng, S. Cao, S. Yuan, and G. Ma, Complementary terahertz absorption and inelastic neutron study of the dynamic anisotropy contribution to zone-center spin waves in a canted antiferromagnet $NdFeO_3$, Phys. Rev. B **90**, 054413 (2014).

[35] J. Jiang, Z. Jin, G. Song, X. Lin, and G. Ma, Dynamical spin reorientation transition in $NdFeO_3$ single crystal observed with polarized terahertz time domain spectroscopy, Appl. Phys. Lett. **103**, 062403 (2013).

[36] X. Fu, X. Zeng, D. Wang, H. Chi-Zhang, J. Han, and T. J. Cui, Ultralow temperature terahertz magnetic thermodynamics of perovskite-like $SmFeO_3$ ceramic, Sci. Rep. **5**, 14777 (2015).

[37] K. Zhang, K. Xu, X. Liu, Z. Zhang, Z. Jin, X. Lin, B. Li, S. Cao, and G. Ma, Resolving the spin reorientation and crystal-field transitions in $TmFeO_3$, Sci. Rep. **6**, 23648 (2016).

[38] K. Amelin, U. Nagel, R. S. Fishman, Y. Yoshida, H. Sim, K. Park, J.-G. Park, and T. Rõõm, Terahertz absorption spectroscopy study of spin waves in orthoferrite $YFeO_3$ in a magnetic field, Phys. Rev. B **98**, 174417 (2018).

[39] X. Li, M. Bamba, N. Yuan, Q. Zhang, Y. Zhao, M. Xiang, K. Xu, Z. Jin, W. Ren, G. Ma *et al.*, Observation of Dicke cooperativity in magnetic interactions, Science **361**, 794 (2018).

[40] S. A. Skorobogatov, S. E. Nikitin, K. A. Shaykhutdinov, A. D. Balaev, K. Yu. Terentjev, G. Ehlers, G. Sala, E. V. Pomjakushina, K. Conder, and A. Podlesnyak, Low-temperature spin dynamics in the $TmFeO_3$ orthoferrite with a non-Kramers ion, Phys. Rev. B **101**, 014432 (2020).

[41] S. A. Skorobogatov, K. A. Shaykhutdinov, D. A. Balaev, M. S. Pavlovskii, A. A. Krasikov, and K. Yu. Terentjev, Spin dynamics and exchange interaction in orthoferrite $TbFeO_3$ with non-Kramers rare-earth ion, Phys. Rev. B **106**, 184404 (2022).

[42] S. Baierl, M. Hohenleutner, T. Kampfrath, A. K. Zvezdin, A. V. Kimel, R. Huber, and R. V. Mikhaylovskiy, Nonlinear spin control by terahertz-driven anisotropy fields, Nat. Photon. **10**, 715 (2016).

[43] S. Schlauderer, C. Lange, S. Baierl, T. Ebnet, C. P. Schmid, D. C. Valovcin, A. K. Zvezdin, A. V. Kimel, R. V. Mikhaylovskiy, and R. Hube, Temporal and spectral fingerprints of ultrafast allcoherent spin switching, Nature **569**, 383 (2019).

[44] R. D. Shannon and C. T. Prewitt, Effective ionic radii in oxides and fluorides, Acta Cryst. B **25**, 925 (1969).

[45] R. D. Shannon, Revised effective ionic radii and systematic studies of interatomie distances in halides and chaleogenides, Acta Cryst. A **32**, 751 (1976).

[46] I. S. Lyubutin, T. V. Dmitrieva, and A. S. Stepin, Dependence of exchange interactions on chemical bond angle in a structural series: Cubic perovskite-rhombic orthoferrite-rhombohedral hematite, Zh. Eksp. Teor. Fiz. **115**, 1070 (1999) [J. Exp. Theor. Phys. **88**, 590 (1999)].

[47] J.-S. Zhou and J. B. Goodenough, Intrinsic structural distortion in orthorhombic perovskite oxides, Phys. Rev. B **77**, 132104 (2008).

[48] J.-S. Zhou and J. B. Goodenough, Universal Octahedral-Site Distortion in Orthorhombic Perovskite Oxides, Phys. Rev. Lett. **94**, 065501 (2005).

[49] J. A. Alonso, M. J. Martínez-Lope, M. T. Casais, and M. T. Fernández-Díaz, Evolution of the jahn−teller distortion of MnO_6 octahedra in $RMnO_3$ perovskites (R = Pr, Nd, Dy, Tb, Ho, Er, Y): A neutron diffraction study, Inorg. Chem. **39**, 917 (2000).

[50] J.-S. Zhou, J. A. Alonso, V. Pomjakushin, J. B. Goodenough, Y. Ren, J.-Q. Yan, and J.-G. Cheng, Intrinsic structural distortion and superexchange interaction in the orthorhombic rare-earth perovskites $RCrO_3$, Phys. Rev. B **81**, 214115 (2010).

[51] S.-J. Kim, G. Demazeau, I. Presniakov, and J.-H. Choy, Structural distortion and chemical bonding in $TlFeO_3$: comparison with $AFeO_3$ (A = rare earth), J. Sol. Stat. Chem. **161**, 197 (2001).

[52] S. Smirnova, Normal modes of the $LaMnO_3$ *Pnma* phase: Comparison with La_2CuO_4 *Cmca* phase, Physica B **262**, 247 (1999).

[53] M. N. Illiev, M. V. Abrashev, H.-G. Lee, V. N. Popov, Y. Y. Sun, C. Thomsen, R. L. Meng, and C. W. Chu, Raman spectroscopy of orthorhombic perovskite like $YMnO_3$ and $LaMnO_3$, Phys. Rev. B **57**, 2872 (1998).

[54] A. Chopelas, Single-crystal Raman spectra of $YAlO_3$ and $GdAlO_3$: Comparison to several orthorhombic ABO_3 perovskites, Phys. Chem. Miner. **38**, 709 (2011).

[55] R. Milkus and A. Zaccone, Local inversion-symmetry breaking controls the boson peak in glasses and crystals, Phys. Rev. B **93**, 094204 (2016).

[56] https://www.helmholtz-Berlin.de/pubbin/igama_output?modus=einzel&gid=1691&sprache=de.

[57] K. Holldack and A. J. Schnegg, THz electron paramagnetic resonance/THz spectroscopy at BESSY II, J. Large-Scale Res. Facilities **2**, A51 (2016).

[58] M. Abo-Bakr, J. Feikes, K. Holldack, P. Kuske, W. B. Peatman, U. Schade, G. Wüstefeld, and H.-W. Hübers, Brilliant, Coherent Far-Infrared (THz) Synchrotron Radiation, Phys. Rev. Lett. **90**, 094801 (2003).

[59] T. Kurosawa, Polarization waves in solids, J. Phys. Soc. Jpn. **16**, 1298 (1961).

[60] Focus software, http://www.cemhti.cnrs-orleans.fr/pot/software/focus.html.

[61] F. Gervais, Optical conductivity of oxides, Mater. Sci. Eng. R **39**, 29 (2002).

[62] M. C. Weber, M. Guennou, H. J. Zhao, J. Íñiguez, R. Vilarinho, A. Almeida, J. A. Moreira, and J. Kreisel, Raman spectroscopy of rare-earth orthoferrites $R\mathrm{FeO}_3$ (R = La, Sm, Eu, Gd, Tb, Dy), Phys. Rev. B **94**, 214103 (2016).

[63] S. Geller and E. A. Wood, Crystallographic studies of perovskite-like compounds. I. Rare earth orthoferrites and YFeO_3, YCrO_3, YAlO_3, Acta Crystallogr. **9**, 563 (1956).

[64] M. Marezio and P. D. Dernier, The bond lengths in LaFeO_3, Mater. Res. Bull. **6**, 23 (1971).

[65] W. C. Koehler and E. O. Wollan, Neutron-diffraction study of the magnetic properties of perovskite-like compounds LaBO_3, J. Phys. Chem. Solids **2**, 100 (1957).

[66] R. J. McQueeney, J.-Q. Yan, S. Chang, and J. Ma, Determination of the exchange anisotropy in perovskite antiferromagnets using powder inelastic neutron scattering, Phys. Rev. B **78**, 184417 (2008).

[67] K. Yosida, *Theory of Magnetism* (Springer-Verlag, Berlin, 1996).

[68] M. Eibschütz, S. Shtrikman, and D. Treves, Mössbauer studies of Fe^{57} in orthoferrites, Phys. Rev. **156**, 562 (1967).

[69] S. Stolen, F. Gronvold, H. Brinks, T. Atake, and H. Mori, Heat capacity and thermodynamic properties of LaFeO_3 and LaCoO_3 from $T = 13$ K to $T = 1000$ K, J. Chem. Thermodyn. **30**, 365 (1998).

[70] S. C. Parida, S. K. Rakshit, and Z. Singh, Heat capacities, order-disorder transitions, and thermodynamic properties of rare-earth orthoferrites and rare-earth iron garnets, J. Solid State Chem. **181**, 101 (2008).

[71] S. M. Selbach, J. R. Tolchard, A. Fossdal, and T. Grande, Non-linear thermal evolution of the crystal structure and phase transitions of LaFeO_3 investigated by high temperature x-ray diffraction, J. Solid State Chem. **196**, 249 (2012).

[72] T. Fujii, I. Matsusue, and J. Takada, Superparamagnetic behaviour and induced ferrimagnetism of LaFeO_3 nanoparticles prepared by a hot-soap technique, in *Advanced Aspects of Spectroscopy*, edited by M. A. Farrukh (InTech, Rijeka, 2012), Chap. 13, pp. 373–390.

[73] K. Park, H. Sim, J. C. Leiner,Y. Yoshida, J. Jeong, S.-i. Yano, J. Gardner, P. Bourges, M. Klicpera, V. Sechovský, M. Boehm, and J.-G. Park, Low-energy spin dynamics of orthoferrites AFeO_3 (A = Y, La, Bi), J. Phys.: Condens. Matter **30**, 235802 (2018).

[74] I. Sosnowska and P. Fischer, Refinement of the crystal and magnetic structure of PrFeO_3 AT $T = 8$ K, J. Less Common Met. **111**, 109 (1985).

[75] Y. Nagata, S. Yashiro, T. Mits uhashi, A. Koriyama, Y. Kawashima, and H. Samata, Magnetic properties of $R\mathrm{Fe}_{1-x}\mathrm{Mn}_x\mathrm{O}_3$ (R = Pr, Gd, Dy), J. Magn. Magn. Mater. **237**, 250 (2001).

[76] K. Feldmann, K. Hennig, L. Kaun, B. Lippold, M. M. Lukina, S. Matthies, W. Matz, and E. Warming, Crystal field levels of Pr^{3+} in PrFeO_3 and PrGaO_3 determined by inelastic neutron scattering, Phys. Status Solidi (b) **72**, 817 (1975).

[77] N. E. Massa, K. Holldack, R. Sopracase, V. Ta Phuocc, L. del Campo, P. Echegut, and J. A. Alonso, Identification of spin wave resonances and crystal field levels in simple chromites $R\mathrm{CrO}_3$ (R = Pr, Sm, Er) at low temperatures in the THz spectral region, J. Magn. Magn. Mater. **468**, 294 (2018).

[78] A. P. Malozemoff and R. L.White, Optical spectra of even-electron rare earth ions in the orthoferrites, Solid State Commun. **8**, 665 (1970).

[79] J. Cao, L. I. Vergara, J. L. Musfeldt, A. P. Litvinchuk, Y. J. Wang, S. Park, and S.-W. Cheong, Spin-Lattice Interactions Mediated by Magnetic Field, Phys. Rev. Lett. **100**, 177205 (2008).

[80] N. P. Cheremisinoff, *Handbook of Ceramics and Composites* Taylor & Francis, New York, 1990).

[81] A. Bombik, H. Böhm, J. Kusz, and A. W. Pacyna, Spontaneous magnetostriction and thermal expansibility of TmFeO_3 and LuFeO_3 rare earth orthoferrites, J. Magn. Magn. Mater. **234**, 443 (2001).

[82] K. B. Aring and A. J. Sievers, Role of the ytterbium spins in the spin reorientation in YbFeO_3, J. Appl. Phys. **41**, 1197 (1970).

[83] N. M. Kovtun, A. S. Karnachev, E. E. Soloviev, A. Y. Chevonenkis, and Shemyakov, NMR study of spin reorientation in ErFeO_3 weak ferromagnet, Fiz. Tverd. Tela (Leningrad) **14**, 2150 (1972) [Sov. Phys. Solid State **14**, 1856 (1973)].

[84] S. Venugopalan and M. M. Becker, Raman scattering study of LuFeO_3, J. Chem. Phys. **93**, 3833 (1990).

[85] U. Chowdhury, S. Goswami, A. Roy, S. Rajput, A. K. Mall, R. Gupta, S. D. Kaushik, V. Siruguri, S. Saravanakumar, S. Israel, R. Saravanan, A. Senyshyn, T. Chatterji, J. F. Scott, A. Garg, and D. Bhattacharya, Origin of ferroelectricity in orthorhombic LuFeO_3, Phys. Rev. B **100**, 195116 (2019).

[86] H. J. Zhao, Y. Yang, W. Ren, A-J. Mao, X. M. Chen, and L. Bellaiche, Creating multiferroics with large tunable electrical polarization from paraelectric rare-earth orthoferrites, J. Phys.: Condens. Matter **26**, 472201 (2014).

[87] H. Bilz, G. Benedek, and A. Bussmann-Holder, Theory of ferroelectricity: The polarizability model, Phys. Rev. B **35**, 4840 (1987).

[88] R. Migoni, H. Bilz, and D. Bäuerle, Origin of Raman Scattering and Ferroelectricity in Oxidic Perovskites, Phys. Rev. Lett. **37**, 1155 (1976).

[89] H. Katsura, N. Nagaosa, and A. V. Balatsky, Spin Current and Magnetoelectric Effect in Noncollinear Magnets, Phys. Rev. Lett. **95**, 057205 (2005).

[90] A. Bussmann-Holder, The polarizability model for ferroelectricity in perovskite oxides, J. Phys.: Condens. Matter **24**, 273202 (2012).

[91] R. G. Burns, *Mineralogical Applications of Crystal Field Theory* (Cambridge University Press, London, 1970).

[92] A. M. Balbashov, A. G. Berezin, Yu. V. Bobryshev, P. Yu. Marchukov, I. V. Nikolaev, Ya. Paches, L. Pust, E. G. Rudashevskii, and V. V. Shushpanov, Orthogonal magnetic "impurity" (Fe^{+3} in c positions) in orthoferrite YFeO_3, Zh. Eksp. Teor. Fiz. **102**, 1397 (1992) [Sov. Phys. JETP **75**, 757 (1992)].

[93] M. Mrad, A. Tarhini, and V. Giordano, Absorbance and energy levels for a Fe^{3+} ion in α-$\mathrm{Al}_2\mathrm{O}_3$. Optical pumping applied to a 31 GHz Maser, Eur. Phys. J.: Appl. Phys. **20**, 31001 (2020).

[94] M. Mrad, P.-Y. Bourgeois, M. E. Tobar, Y. Kersalé, and V. Giordano, Analysis of the whispering gallery mode sapphire

Fe^{3+} maser under magnetic field, Eur. Phys. J. **57**, 21005 (2012).

[95] L. S. Kornienko and A. M. Prokhorov, Electronic Paramagnetic Resonance of the Fe^{3+} Ion in Corundum, ZhETF **40**, 1594 (1961) [JETP **13**, 1120 (1961)].

[96] H. F. Symmons and G. S. Bogle, On the exactness of the spin-Hamiltonian description of Fe^{3+} in sapphire, Proc. Phys. Soc. **79**, 468 (1962).

[97] M. Mrad, P. Y. Bourgeois, Y. Kersalé, and V. Giordano, Fe^{3+} paramagnetic ion in α-Al_2O_3 energy levels revisited. Application to a 31 GHz Maser proposal, arXiv:1201.1760v1.

[98] M. G. Zhao and M. Chiu, Analytical expressions for zero-field splittings of 31 ions in low-symmetry fields and their applications, Phys. Rev. B **52**, 10043 (1995).

[99] B. Bleaney and R. S. Trenam, Paramagnetic resonance spectra of some ferric alums, and the nuclear magnetic moment of ^{57}Fe, Proc. R. Soc. A **223**, 15 (1954).

[100] M. G. Zhao and M. Chiu, Substitution site of the Fe^{3+} impurity in crystalline $LiNbO_3$, Phys. Rev. B **49**, 12556 (1994).

[101] https://chem.libretexts.org/Bookshelves/Physical_and_Theoretical_Chemistry_Textbook_Maps/Supplemental_Modules_(Physical_and_Theoretical_Chemistry)/Spectroscopy/Magnetic_Resonance_Spectroscopies/Electron_Paramagnetic_Resonance/EPR_-_Theory.

[102] E. Magome, C. Moriyoshi, Y. Kuroiwa, A. Masuno, and H. Inoue, Noncentrosymmetric structure of $LuFeO_3$ in metastable state, Jpn. J. Appl. Phys. **49**, 09ME06 (2010).

[103] X. Xu and W. Wang, Multiferroic hexagonal ferrites (h-$R$$FeO_3$, R = Y, Dy-Lu): A brief experimental review, Mod. Phys. Lett. B **28**, 1430008 (2014).

[104] A. K. Choquette, C. R. Smith, R. J. Sichel-Tissot, E. J. Moon, M. D. Scafetta, E. Di Gennaro, F. Miletto Granozio, E. Karapetrova, and S. J. May, Octahedral rotation patterns in strained $EuFeO_3$ and other *Pbnm* perovskite films: Implications for hybrid improper ferroelectricity, Phys. Rev. B **94**, 024105 (2016).

[105] E. Bousquet and A. Cano, Non-collinear magnetism in multiferroic perovskites, J. Phys.: Condens. Matter **28**, 123001 (2016).

[106] L. T. Tsymbal, Y. B. Bazaliy, V. N. Derkachenko, V. I. Kamenev, G. N. Kakazei, F. J. Palomares, and P. E. Wigen, Magnetic and structural properties of spin reorientation transitions in orthoferrites, J. Appl. Phys. **101**, 123919 (2007).

[107] Ya. B. Bazaliy, L. T. Tsymbal, G. N. Kakazei and P. E. Wigen, The role of erbium magnetization anisotropy during the magnetic reorientation transition in $ErFeO_3$, J. Appl. Phys. **95**, 6622 (2004).

[108] H. Pinto, G. Shachar, H. Shaked, and S. Shtrikman, Spin reorientation in $ErFeO_3$ single crystals observed by neutron diffraction, Phys. Rev. B **3**, 3861 (1971).

[109] G. Gorodetsky, L. M. Levinson, S. Shtrikman, D. Treves, and B. M. Wanklyn, Direct observation of spin rotation in $ErFeO_3$, Phys. Rev. **187**, 637 (1969).

[110] R. W. Grant and S. Geller, Mechanism of spin reorientation in $ErFeO_3$, Solid State Commun. **7**, 1291 (1969).

[111] R. C. LeCraw, R. Wolf, E. M. Gyorgy, F. B.Hagedorn, J. C. Hensel, and J. P. Remeika, Microwave Absorption near the Reorientation Temperature in The Rare Earth Orthoferrites, J. Appl. Phys. **39**, 1019 (1968).

[112] R. P. Chaudhury, B. Lorenz, C. W. Chu, Ya. B. Bazaliy and L. T. Tsymbal, Lattice strain and heat capacity anomalies at the spin reorientation transitions of $ErFeO_3$ orthoferrite, J. Phys.: Conf. Ser. **150**, 042014 (2009).

[113] G. Gorodetsky, R. M. Hornreich, I. Yaeger, H. Pinto, G. Shachar, and H. Shaked, Magnetic structure of $ErFeO_3$ below 4.5 K, Phys. Rev. B **8**, 3398 (1973).

[114] I. Fita, R. Puzniak, E. E. Zubov, P. Iwanowski, and A. Wisniewski, Temperature-driven spin switching and exchange bias in the ErFeO3 ferrimagnet, Phys. Rev. B **105**, 094424 (2022).

[115] V. N. Derkachenko, A. M. Kadomtseva, V. A. Timofeeva, and V. A. Khokhlov, Temperature hysteresis of the magnetization in orthoferrites at the compensation point, ZhETF Pis. Red. **20**, 236 (1974) [JETP Lett. **20**, 104 (1974)].

[116] T. N. Stanislavchuk, Yazhong Wang, S.-W. Cheong, and A. A. Sirenko, Far-IR magnetospectroscopy of magnons and electromagnons in $TbFeO_3$ single crystals at low temperatures, Phys. Rev. B **95**, 054427 (2017).

[117] T. N. Stanislavchuk, Yazhong Wang, Y. Janssen, G. L. Carr, S.-W. Cheong, and A. A. Sirenko, Magnon and electromagnon excitations in multiferroic $DyFeO_3$, Phys. Rev. B **93**, 094403 (2016).

[118] R. V. Mikhaylovskiy, E. Hendry, V. V. Kruglyak, R. V. Pisarev, Th. Rasing, and A. V. Kimel, Terahertz emission spectroscopy of laser-induced spin dynamics in $TmFeO_3$ and $ErFeO_3$ orthoferrites in $ErFeO_3$, Phys. Rev. B **90**, 184405 (2014).

[119] R. V. Mikhaylovskiy, T. J. Huisman, V. A. Gavrichkov, S. I. Polukeev, S. G. Ovchinnikov, D. Afanasiev, R. V. Pisarev, Th. Rasing, and A. V. Kimel, Resonant Pumping of *d*-*d* Crystal Field Electronic Transitions as a Mechanism of Ultrafast Optical Control of the Exchange Interactions in Iron Oxides, Phys. Rev. Lett. **125**, 157201 (2020).

[120] M. P. Zic, Wesley T. Fuhrman, K. Wang, S. Ran, J. Paglione, and N. P. Butch, Coupled spin waves and crystalline electric field levels in candidate multiferroic $ErFeO_3$, J. Appl. Phys. **130**, 014102 (2021).

[121] G. Deng, P. Guo, W. Ren, S. Cao, H. E. Maynard-Casely,M. Avdeev, and G. J. McIntyre, The magnetic structures and transitions of a potential multiferroic orthoferrite $ErFeO_3$, J. Appl. Phys. **117**, 164105 (2015).

[122] R. V. Mikhaylovskiy, T. J. Huisman, R. V. Pisarev, Th. Rasing, and A. V. Kimel, Selective Excitation of Terahertz Magnetic and Electric Dipoles in Er^{3+} Ions by Femtosecond Laser Pulses in $ErFeO_3$, Phys. Rev. Lett. **118**, 017205 (2017).

[123] D. L. Wood, L. M. Holmes, and J. P. Remeika, Exchange Fields and Optical Zeeman Effect in $ErFeO_3$, Phys. Rev. **185**, 689 (1969).

[124] D. Afanasiev, J. R. Hortensius, B. A. Ivanov, A. Sasani, E. Bousquet, Y. M. Blanter, R. V. Mikhaylovskiy, A. V. Kimel, and A. D. Caviglia, Ultrafast control of magnetic interactions via light-driven phonons, Nat. Mater. **20**, 607 (2021).

[125] T. Nova, A. Cartella, A. Cantaluppi, M. Först, D. Bossini, R. V. Mikhaylovskiy, A. V. Kimel, R. Merlin, and A. Cavalleri, An effective magnetic field from optically driven phonons, Nat. Phys. **13**, 132 (2017).

[126] M. E. Lines and A. M. Glass, *Principles and Applications of Ferroelectrics and Related Material* (Oxford University Press, Oxford, 2001).